

Optimal Control of Large-Scale Networks using Clustering Based Projections

Nan Xue, *Student Member, IEEE*, Aranya Chakraborty, *Senior Member, IEEE*

Abstract—In this paper we present a set of projection-based designs for constructing simplified linear quadratic regulator (LQR) controllers for large-scale consensus networks. When such networks have tens of thousands of nodes, the design of conventional LQR controllers becomes numerically challenging, and their implementation requires a large number of communication links. Our proposed algorithms bypass these difficulties by clustering the network nodes using structural properties of its closed-loop transfer matrix. The assignment of clusters is defined through a structured projection matrix P , which leads to a significantly lower-dimensional controller design. The reduced-order controller is finally projected back to the original coordinates via an inverse projection. The problem is, therefore, posed as finding the optimal set of clusters or P that minimizes the \mathcal{H}_2 -norm of the error between the transfer matrices of the full-order network with the full-order LQR and with the projected LQR. We derive an upper bound on this error as a function of P , and design a P that minimizes this bound. The design is shown to be implementable by a convenient, hierarchical two-layer control architecture, requiring far less number of communication links than full-order LQR. We illustrate the effectiveness and scalability of our algorithms through simulations.

Index Terms—Clustering, Consensus, Large-Scale Networks, Projection, LQR, \mathcal{H}_2 performance.

I. INTRODUCTION

A vast majority of practical networked dynamic systems (NDS), ranging from power system networks to wireless networks to social or biological networks, consist of several hundreds to thousands of nodes that are spatially distributed over wide geographical spans. Developing tractable control designs for such large complex networks, and implementing those designs through affordable communication, continue to be a challenge for network designers. Conventional state-feedback controllers such as Linear Quadratic Regulators (LQR) involve the computation of large matrix decompositions that can result in detrimental numerical inaccuracies without any guarantee of robustness. They also demand every node in the network to share its state information with every other node, resulting in an impractically large number of communication links. Traditionally, control theorists have addressed the problem of controlling large-dimensional systems by imposing structure on controllers. The most promising approach, for example, started with the idea of decentralized control by Siljak [1], followed by techniques such as singular perturbation theory [2], [3], balanced truncation [4], [5], [6], and ν -gap reduction

[7] among others. These methods aim to simplify the design of controllers for large systems by exploiting weak coupling between their state variables, and by ignoring states that are ‘less important’ than others. The trade-off, however, is that the resulting controllers are often agnostic of the natural coupling between the states, especially the coupling between the closed-loop states, since many of these couplings were forcibly eliminated to facilitate the design itself. Therefore, extending these methods to facilitate controller designs for networks, especially to NDS whose states may be defined over highly structured topologies such as clustering, is quite difficult. A significant literature exists on controllability and observability properties of NDS [8], [9]. But the literature for developing tangible and yet simple low-dimensional controllers that satisfy global stability and dynamic performance requirements of very large NDS is still, unfortunately, very sparse. Ideas on aggregate control [10], *glocal* control [11] and hierarchical control [12], [13] have recently been proposed to address this challenge. The goal of these designs, however, is to guarantee global closed-loop stability by modular tuning of local controller gains; their degrees of freedom for guaranteeing a desired closed-loop performance can be limited.

To bridge this gap, in this paper we propose a set of algorithms for clustering the states of an n -dimensional node- and edge-weighted consensus network into $r > 0$ distinct, non-overlapping groups. We assume n to be a large positive integer, and $r \ll n$ to be a given design parameter. The grouping is defined by a structured projection matrix P whose elements denote the identity of nodes in the clusters, weighted by certain projection weights. The design, thereafter, consists of three steps. First, for the full-order network an n -dimensional LQR controller is defined for any given choice of Q and R . We refer to this controller as the *benchmark* LQR. Second, the projection matrix P is used to construct an r -dimensional reference model for which an r -dimensional LQR controller is designed. The design matrices for this reduced-order controller, however, are not free; they are constrained by being related to Q and R through P . Finally, this reduced-order controller is projected back to the full-order network by the inverse projection P^T . The main problem is then to find a projection matrix P that minimizes the \mathcal{H}_2 -norm of the error between the transfer matrices of the full-order network with the benchmark LQR controller and with the projected LQR controller.

This problem by itself, however, is non-convex. So as a relaxation we first derive an upper bound on the error norm, and then design a P that minimizes this bound. Three distinct variants of the design are proposed. In the first case, we

N. Xue and A. Chakraborty are with the Department of Electrical and Computer Engineering, North Carolina State University, Raleigh, NC, 27695 USA, e-mail: nxue@ncsu.edu, achakra2@ncsu.edu

The work is supported partly by the US National Science Foundation (NSF) under grant ECCS 1054394.

optimize over cluster assignment while keeping the projection weights fixed, and establish that this minimization can be posed as an unsupervised clustering problem. We use weighted k-means [14] to solve this minimization. In the second case, we fix the cluster identities, and optimize over the projection weights. We show that the same minimization can now be posed as solving the Z -eigenvalue of a tensor [15]. In the third case, we propose an iterative method to optimize over both cluster assignment and projection weights. The controllers resulting from all these three clustering algorithms are shown to be implementable by a convenient, hierarchical two-layer control architecture, requiring far less number of communication links than full-order LQR as well as sparsity-promoting LQR [16]. We illustrate the effectiveness and scalability of our algorithms through simulations of consensus networks whose numbers of nodes range from 500 to 10000.

Recently, [17] and [18] have used structural projection-based ideas for model reduction of large networks, but not for control designs. Attention has also been drawn to designing LQR controllers for large systems by finding low-rank solutions of algebraic Riccati equations [19]. However, like most Krylov subspace-based reduction methods such as in [6], the controller in [19] is unstructured, and hence demands as many communication links as the full-order LQR itself. Distributed controllers using model matching [20], sparsity-promoting LQR in [16] and structured LQR in [21] promise to reduce the communication density, but their designs inherit the same dimensionality as the full-order design. Unlike all of these methods, the novelty of our algorithm is in the facilitation of closed-loop control from the perspective of both design and implementation. The recent papers [22], [23] also address both goals, but the dimensionality of their controllers is subject to the sparsity structure of the open-loop network while our design does not necessarily require any such sparsity. The basic rationale behind our approach is to exploit the clustering structure of the controllability Gramian of the closed-loop system with LQR state-feedback control. Moreover, our control scheme is derived on the grounds of clustering, which also opens up further opportunities in consummating control theory with machine learning and computer science.

Preliminary results on the first design have been presented in the recent conference paper [24], but only for specific Q and R , and without detailed illustrations of the computational simplifications. The designs reported in this journal version, on the other hand, are much more general with more complete proofs and illustrations. The second and third design problems are completely new. The remainder of the paper is organized as follows. Section II reviews some fundamental definitions and results from graph theory, which are later borrowed to formulate the problem of clustering-based optimal control in Section III. Section IV justifies the well-posedness of the problem. Section V presents the derivation of the error bound, and poses the clustering algorithm based on the weighted k-means optimization. The design for clustering weight and the iterative algorithm are discussed in Section VI. Validations of all the algorithms are illustrated via simulations in Section VII. Section VIII concludes the paper.

Notation We will use the following notations throughout this paper:

| | |
|---|--|
| $ m $ | absolute value of a scalar m |
| $ \mathcal{S} _c$ | cardinality of a set \mathcal{S} |
| $\mathbf{1}_n$ | column vector of size n with all 1 entries |
| I_k | identity matrix of size k |
| $M_{i,j}$ | the $(i,j)^{th}$ entry of a matrix M |
| $diag(m)$ | diagonal matrix with vector m on its principal diagonal |
| $M \otimes N$ | Kronecker product of M and N |
| $M \circ N$ | Hadamard product of M and N , i.e. $[M \circ N]_{i,j} = M_{i,j} N_{i,j}$ |
| $tr(M)$ | trace operation on a matrix M |
| $ker(M)$ | kernel of a matrix M |
| $\ M\ _F$ | Frobenius norm of a matrix M , i.e. $\ M\ _F = \sqrt{tr(MM^T)}$ |
| $\bar{\sigma}(M), \bar{\lambda}(M)$ | largest singular value, or eigenvalue with largest real part of a matrix M |
| $\underline{\sigma}(M), \underline{\lambda}(M)$ | smallest singular value, or eigenvalue with smallest real part of a matrix M |
| $\bar{v}(M)$ | right eigenvector of $\bar{\lambda}(M)$ |

Given a matrix $M = [m_1, \dots, m_n] \in \mathbb{R}^{n \times n}$, its vector form is defined by $vec(M) = [m_1^T, \dots, m_n^T]^T$, with the inverse operation defined by $unvec(vec(M)) = M$. A transfer matrix is defined as $g(s) = C(sI - A)^{-1}B + D$, with a realization form of $g(s) = \begin{bmatrix} A & B \\ C & D \end{bmatrix}$. For $A = A^T$, $g(s)$ is stable if $A \prec 0$, or semi-stable if $A \preceq 0$. Furthermore, the \mathcal{H}_2 and \mathcal{H}_∞ norms of a stable transfer matrix $g(s)$ are defined by $\|g(s)\|_{\mathcal{H}_2} = \sqrt{\int_{-\infty}^{\infty} tr[g^*(t)g(t)]dt} = \sqrt{\frac{1}{2\pi} \int_{-\infty}^{\infty} tr[g^*(j\omega)g(j\omega)]d\omega}$ and $\|g(s)\|_{\mathcal{H}_\infty} = \sup_{\omega} \bar{\sigma}[g(j\omega)]$.

II. PRELIMINARIES

We briefly recall a few results from algebraic graph theory that will be used in this paper. A graph $\mathcal{G} = (\mathcal{V}, \mathcal{E})$ is defined over a node (vertex) set $\mathcal{V} = \{1, \dots, n\}$ and an edge set $\mathcal{E} \subset \mathcal{V} \times \mathcal{V}$, which contains two-element subsets of \mathcal{V} . If $\{i, j\} \in \mathcal{E}$, we call nodes i and j adjacent, and denote the relation by $i \sim j$, or simply ij . The set of nodes adjacent to $i \in \mathcal{V}$ is noted by $\mathcal{N}_i = \{j \in \mathcal{V} | i \sim j\}$. In this paper, \mathcal{G} is assumed to be undirected, which implies ij is equivalent to ji , and there are no loops or multiple edges between nodes. In addition, every node $i \in \mathcal{V}$ is supposed to have a real-valued node-weight $m_i > 0$. And every edge $ij \in \mathcal{E}$ has a real-valued edge-weight $a_{ij} = a_{ji} > 0$. The diagonal degree matrix $D(\mathcal{G}) \in \mathbb{R}^{n \times n}$ is defined by $D(\mathcal{G})_{i,i} = \sum_{j \in \mathcal{N}_i} a_{ij}$. The symmetric adjacency matrix $A(\mathcal{G}) \in \mathbb{R}^{n \times n}$ is defined as $A(\mathcal{G})_{i,j} = a_{ij}$, if $i \sim j$, and $A(\mathcal{G})_{i,j} = 0$ otherwise. The edge-weighted graph Laplacian matrix, defined as $L(\mathcal{G}) = D(\mathcal{G}) - A(\mathcal{G})$, is symmetric positive-semidefinite. We assume that \mathcal{G} is connected, which implies that the eigenvalues of $-L(\mathcal{G})$ are ordered as $0 = \lambda_1 > \lambda_2 \geq \dots \geq \lambda_n$. The eigenvector corresponding to λ_1 is $v_1 = \frac{1}{\sqrt{n}} \mathbf{1}_n$. The node- and edge-weighted Laplacian matrix is defined by $L_M(\mathcal{G}) = M^{-1}L(\mathcal{G})$, where $M = diag([m_1, \dots, m_n])$ is the matrix of node weights.

III. PROBLEM FORMULATION

Consider a LTI system defined over a connected, node- and edge-weighted graph $\mathcal{G} = (\mathcal{V}, \mathcal{E})$, $\mathcal{V} = \{1, \dots, n\}$ as

$$\begin{cases} \dot{x}_M(t) = -L_M(\mathcal{G})x_M(t) + B_M u(t) + B_{dM} d(t) \\ y(t) = C_M x_M(t) \end{cases}, \quad (1)$$

where $x_M(t) \in \mathbb{R}^n$ and $u(t) \in \mathbb{R}^m$ represent the vector of state and control variables, and $d(t) \in \mathbb{R}^{n_b}$ is a disturbance input entering into the network through one or more designated nodes. $L_M(\mathcal{G}) \in \mathbb{R}^{n \times n}$ is the node- and edge-weighted Laplacian matrix defined in Section II, $B_M \in \mathbb{R}^{n \times m}$ is the control input matrix, $C_M \in \mathbb{R}^{n \times n}$ is the output matrix, and $B_{dM} \in \mathbb{R}^{n \times n_b}$ is the disturbance input matrix. Note that $L_M \neq L_M^T$. We use a coordinate transformation $x = M^{\frac{1}{2}} x_M$ to convert (1) into

$$\begin{cases} \dot{x}(t) = Ax(t) + Bu(t) + Bd d(t), & x(0) = x_0 \\ y(t) = Cx(t) \end{cases}, \quad (2)$$

where $A = A^T = -M^{-\frac{1}{2}} L(\mathcal{G}) M^{-\frac{1}{2}}$, $B = M^{\frac{1}{2}} B_M$, $B_d = M^{\frac{1}{2}} B_{dM}$ and $C = C_M M^{-\frac{1}{2}}$. By this transformation, A becomes symmetric such that the right and left eigenspace of A coincide, which implies, for later interest of derivation, $\bar{\lambda}(A) = 0$ and $\bar{v}(A) = \frac{1}{\sqrt{\text{tr}(M)}} M^{\frac{1}{2}} \mathbf{1}_n$. In the following, we will refer to $\bar{v}(A)$ simply as \bar{v} .

In this paper, we consider an LQR design for (2), and assume $C = I_n$ for a full-state feedback. Given two real-valued matrices $Q = Q^T \succeq 0$ and $R = R^T \succ 0$, the LQR problem is posed as finding a feedback law $u(t) = -Kx(t)$ such that the cost function

$$J := \int_0^\infty [x^T(t)Qx(t) + u^T(t)Ru(t)]dt \quad (3)$$

is minimized. The expression (3), also known as the infinite-horizon continuous-time LQR, can be solved by the following algebraic Riccati equation (ARE)

$$A^T X + XA + Q - XGX = 0, \quad (4)$$

where $G = BR^{-1}B^T$, and the feedback matrix can be found through $K = R^{-1}B^T X$. For such a solution X to exist, that is to maintain the well-posedness of the LQR design, we will adhere to the following assumption throughout this paper.

Assumption III.1. Denote $Q = Q^{\frac{1}{2}} Q^{\frac{T}{2}}$ and $R^{-1} = R^{-\frac{1}{2}} R^{-\frac{T}{2}}$. Assume $(Q^{\frac{T}{2}}, A)$ is detectable, and $(A, BR^{-\frac{1}{2}})$ is stabilizable.

According to [7], the assumption above guarantees a unique stabilizing solution $X = X^T \succeq 0$. The closed-loop transfer matrix (TM) from the disturbance d to state x can then be written as

$$g(s) := (sI_n - A + BK)^{-1} B_d. \quad (5)$$

The model above represents the full-order closed-loop system equipped with the full-order LQR control. However, unlike design in [25], we do not intend or require to approach this controller design in full dimension, especially when \mathcal{G} consists of thousands to tens of thousands of nodes, which makes both

the design and implementation of $u = Kx$ very difficult. Therefore, we define a projection strategy to repose this control problem using a reduced-order system as follows.

Definition III.2. Given an integer r , where $0 < r \leq n$, and a non-zero vector $w \in \mathbb{R}^n$, define r non-empty, distinct, and non-overlapping subsets of the node set $\mathcal{V} = \{1, \dots, n\}$, respectively denoted as $\mathcal{I} = \{\mathcal{I}_1, \dots, \mathcal{I}_r\}$, such that $\mathcal{I}_1 \cup \dots \cup \mathcal{I}_r = \mathcal{V}$. Also define a projection matrix $P \in \mathbb{R}^{r \times n}$ as

$$P_{i,j} := \begin{cases} \frac{w_j}{\|w_{\mathcal{I}_i}\|_2} & j \in \mathcal{I}_i \\ 0 & \text{otherwise} \end{cases}, \quad (6)$$

where $w_{\mathcal{I}_i} = [w_{\mathcal{I}_i\{1\}}, \dots, w_{\mathcal{I}_i\{|\mathcal{I}_i|\}}]^T$ is non-zero, and $\mathcal{I}_i\{j\}$ denotes the j^{th} element in the set \mathcal{I}_i . Note that $PP^T = I_r$.

The construction of P is shown by the following example.

Example 1. Let $w = [1 \ 1 \ 1 \ 2 \ 1 \ 1 \ 1 \ 1 \ 1 \ 1]^T$, $\mathcal{I}_1 = \{1, 2\}$, $\mathcal{I}_2 = \{3, 4, 5\}$ and $\mathcal{I}_3 = \{6, 7, 8, 9, 10\}$. Then,

$$P = \begin{bmatrix} \frac{1}{\sqrt{2}} & \frac{1}{\sqrt{2}} & 0 & 0 & 0 & 0 & 0 & 0 & 0 & 0 \\ 0 & 0 & \frac{1}{\sqrt{6}} & \frac{2}{\sqrt{6}} & \frac{1}{\sqrt{6}} & 0 & 0 & 0 & 0 & 0 \\ 0 & 0 & 0 & 0 & 0 & \frac{1}{\sqrt{5}} & \frac{1}{\sqrt{5}} & \frac{1}{\sqrt{5}} & \frac{1}{\sqrt{5}} & \frac{1}{\sqrt{5}} \end{bmatrix}.$$

We next define a reduced-order model

$$\begin{cases} \dot{\tilde{x}}(t) = \tilde{A}\tilde{x}(t) + \tilde{B}\tilde{u}(t) + \tilde{B}_d d(t), & \tilde{x}(0) = \tilde{x}_0 \\ \tilde{y}(t) = \tilde{C}\tilde{x}(t) \end{cases}, \quad (7)$$

where $\tilde{A} := PAP^T \in \mathbb{R}^{r \times r}$, $\tilde{B}_d := PB_d \in \mathbb{R}^{r \times n_b}$ and $\tilde{C} := PCP^T = I_r$ with P defined as in (6). For this system $\tilde{x} \in \mathbb{R}^r$ is the state and \tilde{u} is the control input. Let $\tilde{Q} := PQP^T \in \mathbb{R}^{r \times r}$ and $\tilde{G} := PGP^T \in \mathbb{R}^{r \times r}$. Let \tilde{B} and \tilde{R} be defined such that $\tilde{B}\tilde{R}^{-1}\tilde{B}^T := \tilde{G} \in \mathbb{R}^{r \times r}$. Note that the quantities \tilde{u} , \tilde{B} and \tilde{R} can have any dimension as long as $\tilde{B}\tilde{u} \in \mathbb{R}^r$, and $\tilde{u}^T \tilde{R} \tilde{u}$ is a scalar. An LQR problem for the reduced-order model (7) is then posed as to minimize

$$\tilde{J} := \int_0^\infty [\tilde{x}^T(t)\tilde{Q}\tilde{x}(t) + \tilde{u}^T(t)\tilde{R}\tilde{u}(t)]dt \quad (8)$$

with respect to $\tilde{u}(t) = -\tilde{K}\tilde{x}(t)$. Here the feedback matrix $\tilde{K} = \tilde{R}^{-1}\tilde{B}^T \tilde{X}$ corresponds to the solution $\tilde{X} \in \mathbb{R}^{r \times r}$ of the reduced-order ARE of (8), which is written as

$$\tilde{A}^T \tilde{X} + \tilde{X} \tilde{A} + \tilde{Q} - \tilde{X} \tilde{G} \tilde{X} = 0. \quad (9)$$

Given the five matrices $(\tilde{A}, \tilde{B}, \tilde{Q}, \tilde{R}, P)$, one can compute $(\tilde{A}, \tilde{Q}, \tilde{G})$, solve (9) for \tilde{X} , and thereafter project it back to its original coordinates through the inverse projection

$$\hat{X} = P^T \tilde{X} P.$$

This *projected controller* can then be implemented in the full-order model (2) using $u = -R^{-1}B^T \hat{X}x$, which implies that in this case the effective feedback gain matrix is $\hat{K} = R^{-1}B^T \hat{X}$. Therefore, the full-order closed-loop system implemented with the projected controller can be written as

$$\hat{g}(s) := (sI_n - A + B\hat{K})^{-1} B_d. \quad (10)$$

Using definitions (5) and (10), we next state our main problem of interest:

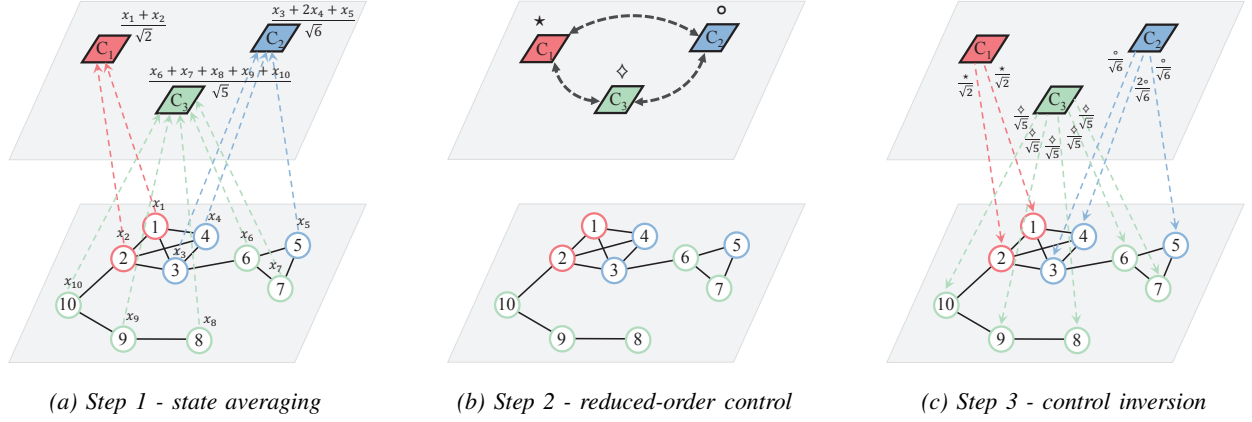


Figure 1: Cyber-physical architecture for implementing the feedback control in Example 2. Solid lines represent physical connections, while dashed lines represent communication links. C_1 , C_2 , C_3 are coordinators for clusters 1, 2 and 3. Network nodes with the same color are assigned to the same coordinator.

Problem Statement: Given system (2) and an integer $r > 0$, find a clustering strategy \mathcal{I} and a non-zero vector w such that the corresponding projection matrix P minimizes $\|g(s) - \hat{g}(s)\|_{\mathcal{H}_2}$. However, this minimization is non-convex. Our main contribution in this paper, therefore, is to derive an upper bound for $\|g(s) - \hat{g}(s)\|_{\mathcal{H}_2}$ as a function of P , and thereafter design P to minimize this bound.¹

We address this problem in two ways. In Section V, we find the clustering set \mathcal{I} for a fixed w . In Section VI, we solve for the weight vector w for fixed \mathcal{I} . We also propose to combine these two approaches by an iterative algorithm in Section VI.

An important point to note is that the physical meaning of the state $\tilde{x}(t)$ of the reduced-order model (7) has no relation to that of the state $x(t)$ of the full-order model (2). Nor is \tilde{A} expected to be a Laplacian matrix as was the case in [17] or [18]. This is a key difference of our design from traditional model-reduction based designs where the reduced-order state vector is typically a direct projection of the full-order state vector. The projection in our design is rather applied on the controller \tilde{X} instead of $x(t)$ since our goal is to compare two closed-loop systems, not their open-loop behavior. Three natural benefits of this approach are:

1. *Tractability:* In Section V we will show that the projection matrix P can be computed by using only a κ -dimensional subspace of the full-order closed-loop controllability Gramian of the model (2), where $\kappa < n$. Ideally, one may choose κ to be at most r . The controller \tilde{X} is also r -dimensional. Therefore, if $r \ll n$ the design becomes significantly more tractable than an n -dimensional LQR controller², especially when n is a very large number.

2. *Simplicity in implementation:* The projected controller $\tilde{X} = P^T \tilde{X} P$ is a structured r -ranked matrix. This results in a sequential two-layer hierarchical control architecture. The

bottom layer consists of the physical network with physical actuations of control signals. The top layer, on the other hand, represents the computation of the averaged states, and the control input $u(t)$. The two layers are connected via at most n communication links at any time t . This architecture is illustrated by the following example.

Example 2. (Continued) The clusters assigned by \mathcal{I}_1 , \mathcal{I}_2 and \mathcal{I}_3 are shown by the red, blue and green circles in Fig. 1. The implementation of a feedback action $u(t) = -R^{-1}B^T \tilde{X}x(t) = -R^{-1}B^T P^T \tilde{X}Px(t)$ for any time instant t is illustrated in this figure through the following three steps:

- *Step 1 - Projection to reduced-order space (Px):* Since P is structured as in (6), the multiplication Px amounts to r aggregate states, which are weighted averages of the actual states. Note, however, that these aggregate states are not the same as \tilde{x} in (7). In terms of implementation, this means that every node in a cluster will transmit their individual state measurements to a designated computing station assigned for each cluster. We refer to these computing stations as coordinators. Each cluster will have a unique coordinator. In Fig. 1, these coordinators are denoted by C_1 , C_2 and C_3 . Each coordinator receives states from its clustered nodes, and computes the weighted averaged state $P_{i,:}x$ for its cluster, $i = 1, 2, \dots, r$.
- *Step 2 - Reduced-order control ($\tilde{X}Px$):* Next, the coordinators communicate with each other, and exchange the weighted averaged states to compute the r -dimensional reduced-order feedback signal $\tilde{X}Px = [\star \quad \circ \quad \diamond]^T$. The computation, however, is completely distributed, meaning C_1 only computes \star , C_2 only computes \circ , and C_3 only computes \diamond .
- *Step 3 - Inverse projection ($R^{-1}B^T P^T \tilde{X}Px$):* The final step of the implementation consists of two sub-steps. First, each coordinator shares its computed value of \star , \circ and \diamond at time t with other coordinators. After that each coordinator computes a unique control signal for each node in its own cluster at time t using linear combinations of \star , \circ and \diamond following from the rows of $R^{-1}B^T P^T$. The pre-multiplication of $\tilde{X}Px$ with $R^{-1}B^T P^T$ represents

¹The initial condition for the reduced-order model (7) does not need to be related to that of the full-order model (2). Our goal is to compare (5) and (10), both of which have zero initial conditions.

²Note that the control input \tilde{u} for the reduced-order model (7) is completely hypothetical. We need to define this quantity only to facilitate the formulation of (9). In reality, one does not need to compute $\tilde{u}(t)$ or \tilde{K} , but only \tilde{X} which follows from (9). Similarly, it is not necessary to define \tilde{B} and \tilde{R} individually as the solution of (9) is only impacted by \tilde{G} .

the inverse projection of the control signal to the full-order system. In the special case when $R^{-1}B^T = I_n$, coordinators do not need to exchange their results from Step 2, and can compute the control input for their cluster nodes by simple scaling of \star , \circ or \diamond based on corresponding elements of w . For this example, $u^T =$

$$\left[\begin{array}{cccccccccccc} \star & \star & \vdots & \circ & \circ & \vdots & \circ & \circ & \circ & \circ & \circ & \circ \\ \sqrt{2} & \sqrt{2} & \vdots & \sqrt{6} & \sqrt{6} & \vdots & \sqrt{5} & \sqrt{5} & \sqrt{5} & \sqrt{5} & \sqrt{5} & \sqrt{5} \end{array} \right].$$

From a cyber-physical perspective, the two-layer control implementation described in Example 2 results in a much sparser communication network with at most $n + \binom{n}{2}$ links compared to a direct LQR controller for the full-order system which would require $\binom{n}{2}$ number of links. This reduction, combined with standard networking protocols such as multi-casting [26], makes the implementation of our proposed controller very convenient and cheap. For example, for the 10-node network in Example 2, a full-order LQR controller would need $\binom{10}{2} = 45$ bidirectional communication links. For the two-layer implementation, however, we need only 13 bidirectional links, 10 of them between nodes and coordinators, and 3 of them between coordinators. The design, therefore, tremendously facilitates sparsity in communication, especially when $n \gg r$.

3. *Data privacy*: The states of all nodes in a cluster are transmitted to only the coordinator designated to that cluster. The coordinators only have to exchange weighted averages of those states. Therefore, no coordinator can infer the individual states of nodes from other clusters. The design, therefore, preserves data privacy.

We next describe the theoretical derivation of our controllers, and prove that they guarantee closed-loop stability. We start off by presenting the well-posedness of the projected controller \hat{X} .

IV. WELL-POSEDNESS RESULTS

In this section we prove the existence and uniqueness of the solution \hat{X} of the reduced-order ARE (9). We also prove that the LQR controller when projected to full dimension is stabilizing, i.e., eigenvalues of $A - B\hat{K}$ are all in the left half-plane. To establish the solvability and stabilizability conditions for \hat{X} , we start by examining the stability of the open-loop system (7) as follows.

Proposition IV.1. *The reduced-order system (7) is semi-stable (or stable) if and only if $w \in \text{span}(\bar{v})$ (or $w \notin \text{span}(\bar{v})$).*

Proof. The semi-stability of (7) has been previously shown in [18] for $w = \bar{v}$. Here we generalize w to any non-zero vector. Denote the complement of the projection matrix P by $U \in \mathbb{R}^{(n-r) \times n}$, such that $D = [P^T \ U^T]^T$ is unitary, i.e. $DD^T = I_n$. By so, $\tilde{A} = PAP^T$ becomes a leading principal of the matrix

$$DAD^T = \begin{bmatrix} PAP^T & PAU^T \\ UAP^T & UAU^T \end{bmatrix},$$

which is similar to A . Given the leading principal of a symmetric positive-definite (or-semidefinite) matrix still being positive-definite (or-semidefinite), it follows that $\tilde{A} \preceq 0$. Moreover, from Definition III.2, P is defined over w such that $P^T Pw = w$. Thus for any non-zero vector $v \in \mathbb{R}^r$,

$PAP^T v = 0$ if and only if $P^T v \in \text{span}(\bar{v})$. By pre-multiplying both side of $P^T v \in \text{span}(\bar{v})$ by $P^T P$, we have $P^T v \in \text{span}(\bar{v})$ equivalent to $P^T v \in \text{span}(P^T P\bar{v})$. This means that the two spaces $\text{span}(P^T P\bar{v})$ and $\text{span}(\bar{v})$ are identical, and thus $w \in \text{span}(\bar{v})$. Therefore, \tilde{A} will preserve the zero eigenvalue of A if and only if $w \in \text{span}(\bar{v})$, or be strictly negative-definite otherwise. \square

The next theorem shows the existence of \hat{X} for the reduced-order ARE (9) for any w and \mathcal{I} .

Theorem IV.2. (Solvability of reduced-order ARE) *If Assumption III.1 holds, then (9) is guaranteed with a unique stabilizing solution $\hat{X} = \hat{X}^T \succeq 0$.*

Proof. For $Q \succeq 0$ and $G \succeq 0$, similar to \tilde{A} in the proof of Proposition IV.1, we have both $\tilde{Q} \succeq 0$ and $\tilde{G} \succeq 0$. Let v be any eigenvector of \tilde{A} , and by definition $v \neq 0$. Recall that $(\tilde{Q}^{\frac{T}{2}}, \tilde{A})$ is detectable if and only if for all λ and v that $\tilde{A}v = \lambda v$ and $\lambda \geq 0$, $\tilde{Q}^{\frac{T}{2}}v \neq 0$. By Proposition IV.1, \tilde{A} can have one zero eigenvalue, with the corresponding eigenvector being $P\bar{v}$ for $w \in \text{span}(\bar{v})$. Under this situation, $\bar{v}^T P^T \tilde{Q} P \bar{v} = \bar{v}^T Q \bar{v} \neq 0$ since $(\tilde{Q}^{\frac{T}{2}}, \tilde{A})$ is detectable. If $w \notin \text{span}(\bar{v})$, \tilde{A} is strictly negative, which means $(\tilde{Q}^{\frac{T}{2}}, \tilde{A})$ is trivially detectable. Likewise, $v^T \tilde{B} \tilde{R}^{-1} \tilde{B}^T v \neq 0$ holds for both $v = P\bar{v}$ or $v \neq P\bar{v}$. Therefore, both stabilizability and detectability are satisfied, and thus (9) guarantees a unique positive-semidefinite solution. \square

To assure that \hat{X} is stabilizing for the transfer matrix $\hat{g}(s)$ in (10), an additional assumption needs to be made:

Assumption IV.3. $w \not\perp \bar{v}$.

Note that this assumption on w is to avoid the situation where $\bar{v} \in \ker(\hat{X})$ such that the state matrix $A - B\hat{K}$ has a zero eigenvalue at \bar{v} , i.e. $(A - B\hat{K})\bar{v} = 0$. Keeping this in mind, in the following, we list three sufficient conditions for the stabilizability of \hat{X} .

Theorem IV.4. (Guaranteed stability I) *The system $\hat{g}(s)$ is strictly stable if $w = \bar{v}$, and \mathcal{I} is an almost equitable partition [27] of the graph \mathcal{G} , which means for $k \neq l$, the edge weight $a_{i,j}$ is equal for all $i \in \mathcal{I}_k$ and $j \in \mathcal{I}_l$.*

Proof. A similarity transformation of $D = [P^T \ U^T]^T$ and D^T on $A - G\hat{X}$ yields

$$D(A - G\hat{X})D^T = \begin{bmatrix} \tilde{A} - \tilde{G}\tilde{X} & PAU^T \\ UAP^T - UG\tilde{X} & UAU^T \end{bmatrix}. \quad (11)$$

From [27], if \mathcal{G} admits an almost equitable partition \mathcal{I} , the corresponding matrix P with $w = \bar{v}$ will satisfy $A^T P^T = P^T F$ for some $F \in \mathbb{R}^{r \times r}$. As a result, $PAU^T = 0$, and thus $\hat{g}(s)$ is stable since $\tilde{A} - \tilde{G}\tilde{X}$ and UAU^T are both Hurwitz given $w = \bar{v}$. \square

The above theorem guarantees closed-loop stability when $w = \bar{v}$, and the clustering set \mathcal{I} must satisfy a very specific structure. In practice, these conditions may be restrictive. To overcome that limitation, we next state an alternative theorem where closed-loop stability can be achieved by imposing a constraint on B and R .

Theorem IV.5. (Guaranteed stability II) Assume that B is a square invertible matrix. Then, $\hat{g}(s)$ is strictly stable if G is similar to αI_n for some $\alpha > 0$.

Proof. Denote the right eigenspace of G by V . Then a coordinate change of V^T and V yields

$$V^T(G\hat{X} + \hat{X}G)V = V^T\hat{X}V \circ [\lambda_i(G) + \lambda_j(G)].$$

Notice that the matrix $[\lambda_i(G) + \lambda_j(G)]$ is positive-semidefinite if and only if its Cholesky decomposition exists. As can be verified from the closed-form expression of Cholesky decomposition, the existence is equivalent to $\lambda_i(G) = \lambda_j(G)$ for $i, j = 1, \dots, n$. That is, G is similar to αI_n for $\alpha = \lambda(G) > 0$. As a result, $G\hat{X} + \hat{X}G$ is positive-semidefinite according to the Schur product theorem. From the matrix majorization property [28], we also have

$$2\bar{\lambda}(A - G\hat{X}) \leq z^T(A + A^T - G\hat{X} - \hat{X}G)z$$

hold for any non-zero vector z , with the RHS being non-positive given $A + A^T \preceq 0$ and $-G\hat{X} - \hat{X}G \preceq 0$. Hence for $\bar{\lambda}(A - G\hat{X})$ to be strictly negative, $z^T A z = 0$ should contradict $z^T G\hat{X} z = 0$. Recall that $z^T A z = 0$ if and only if z is an eigenvector of the zero eigenvalue, namely $z \in \text{span}(\bar{v})$. On the other hand, $z^T G\hat{X} z = 0$ holds if and only if either one of the following three conditions is satisfied: (1) $z \in \ker(P)$, (2) $z \in \ker(G)$, or (3) $Pz \in \ker(\tilde{X})$. Therefore, to prove the contradiction we start by assuming $z^T A z = 0$, i.e., $z \in \text{span}(\bar{v})$. First of all, from Assumption IV.3 we have $w \not\perp \bar{v}$, which means $P\bar{v} \neq 0$ and thus $z \notin \ker(P)$. Similarly given $(A, BR^{-\frac{1}{2}})$ being stabilizable, we have $\bar{v}^T G\bar{v} \neq 0$, i.e. $z \notin \ker(G)$. To this end, the last condition remaining is $z \in \text{span}(\bar{v}) \not\Rightarrow Pz \in \ker(\tilde{X})$ to complete the contradiction. By assuming a non-zero vector $v \in \ker(\tilde{X})$, pre- and post-multiplying (9) with v yields

$$v^T \tilde{A}^T \tilde{X} v + v^T \tilde{X} \tilde{A} v + v^T \tilde{Q} v - v^T \tilde{X} \tilde{G} \tilde{X} v = 0.$$

It can be easily verified that $\ker(\tilde{X})$ is an \tilde{A} -invariant subspace contained in the null-space of \tilde{Q} . Given $z \in \text{span}(\bar{v})$, from the proof of Proposition IV.1 we know that Pz is \tilde{A} -invariant, i.e., Pz is an eigenvector of \tilde{A} , when $w \in \text{span}(\bar{v})$. As a result, $z^T P^T \tilde{Q} P z = z^T Q z \neq 0$ since $(Q^{\frac{T}{2}}, A)$ is detectable. This verifies that Pz is not in the null space of \tilde{Q} , which proves $Pz \notin \ker(\tilde{X})$. Therefore, we conclude that $z^T A z = 0$ contradicts $z^T(G\hat{X} + \hat{X}G)z = 0$, and thus $\hat{g}(s)$ is stable. \square

Remark. Theorem IV.5 holds not only for (2) but for any LTI system with $A = A^T \preceq 0$ and B square invertible. The condition G being similar to αI_n can be achieved by choosing $R = \alpha^{-1} B^T \bar{R} B$ with any unitary \bar{R} , which is equivalent to imposing a weight $\alpha^{-1} \bar{R}$ on Bu directly instead of u for the LQR problem in (3).

The condition in Theorem IV.5 presumes B to be invertible, which limits the number of states to be equal to that of the inputs. This limitation can be bypassed by imposing a restriction on (Q, R) instead, as shown next.

Theorem IV.6. (Conditional stabilizability on Q and R) $\hat{g}(s)$ is strictly stable if $(Q^{\frac{T}{2}}, A)$ is observable and

$$\underline{\sigma}(Q) - 2\bar{\sigma}(X)\bar{\sigma}(G)\bar{\sigma}(E) + \underline{\sigma}(X)^2 \underline{\sigma}(G) > 0 \quad (12)$$

with $E = X - \hat{X}$ denoting the error between the ARE solutions of the full-order system (4) and projected system (9).

Proof. If we restrict Assumption III.1 by letting $(Q^{\frac{T}{2}}, A)$ be observable, the full-order solution X is positive-definite according to [7]. Consider a Lyapunov function $V(x) = x^T X x > 0$, its derivative yields

$$\begin{aligned} \dot{V}(x) &= 2x^T X \dot{x} = 2x^T X(A - G\hat{X})x \\ &= x^T [(A - G\hat{X})^T X + X(A - G\hat{X})]x. \end{aligned}$$

For $\hat{g}(s)$ to be asymptotically stable, $\dot{V}(x)$ needs to be negative, or equivalently

$$(A - G\hat{X})^T X + X(A - G\hat{X}) \prec 0.$$

Using the ARE (4), the LMI above reduces to

$$Q \succ XGE + EGX - XGX,$$

which holds if $\underline{\lambda}(Q) > \bar{\lambda}(XGE + EGX - XGX)$. Notice that the RHS of the eigenvalue inequality follows

$$\bar{\lambda}(XGE + EGX - XGX) \leq \bar{\lambda}(XGE + EGX) + \bar{\lambda}(-XGX),$$

where we have respectively $\bar{\lambda}(XGE + EGX) \leq \bar{\sigma}(XGE + EGX) \leq 2\bar{\sigma}(X)\bar{\sigma}(G)\bar{\sigma}(E)$, and $-\bar{\lambda}(-XGX) = \underline{\sigma}(XGX) \geq \underline{\sigma}(X)^2 \underline{\sigma}(G)$. Incorporating these two upper bounds yields the condition in (12). \square

The following lemma provides a sufficient condition by which (12) can be verified without knowing X .

Lemma IV.7. The stability condition (12) holds if

$$\bar{\sigma}(\hat{X}) \leq \frac{\underline{\sigma}(Q)\underline{\sigma}(G - A)}{\bar{\sigma}(G)\bar{\sigma}(Q + G)} - \frac{\bar{\sigma}(Q + G)}{2\underline{\sigma}(G - A)}. \quad (13)$$

Proof. The proof is presented in the Appendix. \square

In order to meet the stability condition (12), one can select Q and R such that $\underline{\sigma}(Q) \gg \bar{\sigma}(G) > 0$. In practice, this choice of (Q, R) will make the design more robust towards the uncertainties in A and B [31]. As a drawback, a larger Q will also result in a high feedback gain, making the system vulnerable to noise. An alternative to satisfy (12) is to minimize $\bar{\sigma}(E)$. As will be shown in the next section, $\bar{\sigma}(E)$ is proportional to $\|g(s) - \hat{g}(s)\|_{\mathcal{H}_2}$, and thus minimizing it will assist in enlarging the inequality gap in (12). It is also worth mentioning that while the network structure in the model (2) helps in the interpretation of clustering, all the results to be presented next hold for any state matrix $A = A^T$ in (2) that satisfies the well-posedness conditions.

V. \mathcal{H}_2 -CLUSTERING FOR CLOSED-LOOP SYSTEM

In this section, we present our control design assuming that the sufficient conditions for closed-loop stability from either of Theorems IV.4, IV.5 or IV.6 hold.

A. Upper Bound Relaxation

As mentioned before, finding a P that exactly minimizes $\|g(s) - \hat{g}(s)\|_{\mathcal{H}_2}$ is a non-convex problem. To relax this problem, we, therefore, find an upper bound for $\|g(s) - \hat{g}(s)\|_{\mathcal{H}_2}$. We denote the error system by $g_e(s)$, which can be written as

$$g_e(s) := g(s) - \hat{g}(s) = \left[\begin{array}{c|c} \frac{A_e}{C_e} & \frac{B_e}{0} \end{array} \right] = \left[\begin{array}{cc|c} A - GX & & B_d \\ \hline A - G\hat{X} & & -B_d \\ \hline I_n & I_n & 0 \end{array} \right]. \quad (14)$$

From a similarity transformation of $T = \begin{bmatrix} I_n & I_n \\ I_n & 0 \end{bmatrix}$ and $T^{-1} = \begin{bmatrix} 0 & I_n \\ I_n & -I_n \end{bmatrix}$, (14) yields

$$g_e(s) = \left[\begin{array}{c|c} \frac{TA_eT^{-1}}{C_eT^{-1}} & \frac{TB_e}{0} \end{array} \right] = \left[\begin{array}{cc|c} A - G\hat{X} & G(\hat{X} - X) & 0 \\ \hline & A - GX & B_d \\ \hline I_n & 0 & 0 \end{array} \right] = -(sI_n - A + G\hat{X})^{-1}GE(sI_n - A + GX)^{-1}B_d, \quad (15)$$

where $E = X - \hat{X}$. By taking norms on both side of (15), we initially acquire an inequality of

$$\|g_e(s)\|_{\mathcal{H}_2} \leq \|(sI_n - A + G\hat{X})^{-1}G\|_{\mathcal{H}_\infty} \|Eg(s)\|_{\mathcal{H}_2}.$$

Furthermore, by applying the bounded real lemma [7] and the definition of \mathcal{H}_2 norm on the RHS, the norm $\|g_e(s)\|_{\mathcal{H}_2}$ satisfies the following bound,

$$\|g_e(s)\|_{\mathcal{H}_2} \leq \gamma \|E\Phi^{\frac{1}{2}}\|_F, \quad (16)$$

where γ is any positive real number such that a real-valued matrix $\Gamma = \Gamma^T \succeq 0$ exists and satisfies

$$\left[\begin{array}{ccc} \Gamma(A - G\hat{X}) + (A - G\hat{X})^T\Gamma & \Gamma G & I_n \\ G\Gamma & -\gamma I_n & 0 \\ I_n & 0 & -\gamma I_n \end{array} \right] \prec 0,$$

and $\Phi := \Phi^{\frac{1}{2}}\Phi^{\frac{T}{2}} = \int_0^\infty e^{(A-GX)\tau} B_d B_d^T e^{(A-GX)^T\tau} d\tau$ is the solution of the Lyapunov equation

$$(A - GX)\Phi + \Phi(A - GX)^T + B_d B_d^T = 0. \quad (17)$$

Inequality (16) shows that $\|g_e(s)\|_{\mathcal{H}_2}$ is linearly bounded by $\|E\Phi^{\frac{1}{2}}\|_F$. Therefore, one way to minimize $\|g_e(s)\|_{\mathcal{H}_2}$ will be to find a P that minimizes $\|E\Phi^{\frac{1}{2}}\|_F$. By doing so, $\|E\|_F$ can also be minimized to some extent since $\|E\|_F \leq \|\Phi^{-\frac{1}{2}}\|_F \|E\Phi^{\frac{1}{2}}\|_F$. In the literature, this type of minimization has been attempted (see [19] and the references therein) under the assumption that P is unstructured, or more specifically P is an r -dimensional Krylov subspace from $\mathcal{K}(A, Q^{\frac{1}{2}}, r) = [Q^{\frac{1}{2}} \quad A Q^{\frac{1}{2}} \quad \dots \quad A^{r-1} Q^{\frac{1}{2}}]$. By this assumption, E can be found as an explicit function of P associated with a Householder transformation. In our case, however, P has a structure as in (6), due to which this explicit functional relationship does not hold anymore. We, therefore, apply perturbation theory of ARE to further relax the bound in (16), and derive a new upper bound on $\|E\Phi^{\frac{1}{2}}\|_F$ as a function of P in the following theorem.

Theorem V.1. Denote $\xi = \|(I_n - P^T P)\Phi^{\frac{1}{2}}\|_F$. The norm of the weighted error $E\Phi^{\frac{1}{2}}$ satisfies the inequality

$$\|E\Phi^{\frac{1}{2}}\|_F \leq f(\xi) = 2n\epsilon_1\epsilon_2\xi + n\epsilon_1\|Q\|_F\xi^2, \quad (18)$$

where n is the system order, and $\epsilon_1 = \frac{\|\Phi^{-\frac{1}{2}}\|_F}{\sigma[\Phi^{-\frac{1}{2}}(A - GX)\Phi^{\frac{1}{2}}]} > 0$ and $\epsilon_2 = \frac{\sqrt{\tau}\bar{\sigma}(Q+G)}{2\sigma(G-A)}\|A\|_F\|\Phi^{\frac{1}{2}}\|_F + \|Q\Phi^{\frac{1}{2}}\|_F > 0$ are scalars that are independent of P .

Proof. The proof is presented in the Appendix. \square

From (16) and (18), it follows that $\|g_e(s)\|_{\mathcal{H}_2} \leq \gamma f(\xi)$, so we approach the minimization of $\|g_e(s)\|_{\mathcal{H}_2}$ by minimizing $f(\xi)$ with respect to P . It is worth mentioning that the function $f(\xi)$ is in a very convenient form given that the unknown P is only contained in ξ . Most importantly, $f(\xi)$ is a monotonic function with respect to ξ . As a result, minimization of $f(\xi)$ is equivalent to minimizing the value of ξ as

$$\underset{P}{\text{minimize}} \quad \xi = \|\Phi^{\frac{1}{2}} - P^T P \Phi^{\frac{1}{2}}\|_F. \quad (19)$$

In general, (19) is also an NP-hard problem, but fortunately the specific structure of the objective function in the RHS of (19), together with the structure imposed on P in (6), is such that it can be minimized by tractable algorithms such as weighted k-means. We next show these results as follows.

B. Posing (19) as Weighted k-means Optimization

To establish the equivalency of (19) to the weighted k-means optimization, it is useful to borrow a nominal projection matrix \bar{P} as

$$\bar{P}_{i,j} := \begin{cases} \frac{1}{\|w_{\mathcal{I}_i}\|_2} & j \in \mathcal{I}_i \\ 0 & \text{otherwise} \end{cases}, \quad i = 1, \dots, r. \quad (20)$$

From Definition III.2, \bar{P} satisfies $P = \bar{P}W$, where $W = \text{diag}(w)$. With this notation, we have

$$\Phi^{\frac{1}{2}} - P^T P \Phi^{\frac{1}{2}} = W(\Psi - \bar{P}^T \bar{P} W^2 \Psi), \quad (21)$$

where $\Psi = [\psi_1, \dots, \psi_n]^T$ denotes the matrix $W^{-1}\Phi^{\frac{1}{2}}$. Therefore, the entries of the matrix $\bar{P}^T \bar{P} W^2$ can be found by

$$[\bar{P}^T \bar{P} W^2]_{j,k} = \begin{cases} \frac{w_k^2}{\|w_{\mathcal{I}_i}\|_2^2} & j \in \mathcal{I}_i \text{ \& \& } k \in \mathcal{I}_i \\ 0 & \text{otherwise} \end{cases}$$

for $i = 1, \dots, r$. Thus the j^{th} row of the matrix $\bar{P}^T \bar{P} W^2 \Psi$ can be written as

$$[\bar{P}^T \bar{P} W^2 \Psi]_{j,:} = c_i^T = \frac{\sum_{k \in \mathcal{I}_i} w_k^2 \psi_k^T}{\sum_{k \in \mathcal{I}_i} w_k^2}, \quad (22)$$

for $j \in \mathcal{I}_i$. It is clear from above that for all the index j that are assigned to the same cluster \mathcal{I}_i , c_i^T is a weighted average (or a weighted centroid) of the row vectors ψ_j^T . Moreover, the matrix $\bar{P}^T \bar{P} W^2 \Psi$ will have identical rows for those whose indices are inside the same cluster. Therefore, (19) can be posed as an unsupervised clustering problem

$$\underset{\mathcal{I}_1, \dots, \mathcal{I}_r}{\text{minimize}} \quad \xi^2 = \sum_{j=1}^n w_j^2 \|\psi_j - c_i\|_2^2. \quad (23)$$

The optimization problem in (23) is in the same form as a weighted k-means optimization, which minimizes the Euclidean distance weighted by w_j^2 between each data point ψ_j and its centroid c_i . Thus, data points which are close to each other in the weighted distance are assigned to the same cluster. A standard method for solving this problem is Lloyd's algorithm [14], using which we summarize the weighted k-means clustering for (23) in Algorithm 1. With $\Phi^{\frac{1}{2}} \in \mathbb{R}^{n \times n}$ as the input, the running time of Lloyd's algorithm is $\mathcal{O}(nnrk)$, where k is the total number of iterations.

Algorithm 1: \mathcal{H}_2 closed-loop clustering

Input : $\Phi^{\frac{1}{2}}$, w and r

1 **Initialization:** Assign r random rows from $\Psi = W^{-1}\Phi^{\frac{1}{2}} = [\psi_1, \dots, \psi_n]^T$ as the initial centroids c_1^0, \dots, c_r^0 ;

2 Find initial clustering sets $\mathcal{I}^0 = \{j \rightarrow \mathcal{I}_i^0 \mid \arg\min_{i=1, \dots, r} w_j^2 \|\psi_j - c_i^0\|_2^2, j = 1, \dots, n\}$;

3 Update the centroids: $c_i^0 = \frac{\sum_{j \in \mathcal{I}_i^0} w_j^2 \psi_j}{\sum_{j \in \mathcal{I}_i^0} w_j^2}, i = 1, \dots, r$;

4 $k = 1$;

5 **while** $\mathcal{I}^{k-1} \neq \mathcal{I}^k$ **or within maximum iterations** **do**

6 Update clustering sets $\mathcal{I}^k = \{j \rightarrow \mathcal{I}_i^k \mid \arg\min_{i=1, \dots, r} w_j^2 \|\psi_j - c_i^{k-1}\|_2^2, j = 1, \dots, n\}$;

7 Update the centroids: $c_i^k = \frac{\sum_{j \in \mathcal{I}_i^k} w_j^2 \psi_j}{\sum_{j \in \mathcal{I}_i^k} w_j^2}, i = 1, \dots, r$;

8 $k = k + 1$;

9 **end**

Output: $\mathcal{I} = \mathcal{I}^k$

C. Low-Dimensional Approximation for Φ

We conclude this section with a discussion on the numerical complexities of Algorithm 1, and how these complexities can be resolved by making appropriate approximations on Φ . First, recall the definition of the Hamiltonian matrix

$$H := \begin{bmatrix} A & -G \\ -Q & -A^T \end{bmatrix}. \quad (24)$$

The eigenvalues of H are symmetric about the imaginary axis. Suppose H is diagonalizable and that the columns of the matrix $\begin{bmatrix} Y \\ Z \end{bmatrix}_{2n \times n}$ span the stable invariant subspace of H , i.e.

$$H \begin{bmatrix} Y \\ Z \end{bmatrix} = \begin{bmatrix} Y \\ Z \end{bmatrix} \Lambda^-, \quad (25)$$

where $\Lambda^- = \text{diag}([\lambda_1^-, \dots, \lambda_n^-])$ consists of all the eigenvalues of H in the left-half plane, i.e. $0 > \lambda_1^- > \dots > \lambda_n^-$. The stabilizing solution of ARE can thus be found by $X = ZY^{-1}$ [7]. Then, the first n rows of (25) are expanded as $A - GZY^{-1} = Y\Lambda^-Y^{-1}$, which means Λ^- and the normalized Y are the eigenvalues and right eigenspace of the closed-loop state matrix $A - GX$. Then from the Lyapunov equation (17), we can write Φ directly in terms of Y and Λ^- by [6]

$$\Phi = Y(Y^{-1}B_d B_d^T Y^{-T} \circ \mathcal{C})Y^T, \quad (26)$$

where $\mathcal{C} \in \mathbb{R}^{n \times n}$ is a Cauchy matrix with

$$\mathcal{C}_{i,j} = \left[-\frac{1}{\lambda_i^- + \lambda_j^-} \right],$$

and subsequently obtain $\Phi^{\frac{1}{2}}$ from the Cholesky decomposition. Therefore, to compute the Gramian Φ and then $\Phi^{\frac{1}{2}}$, one will need to compute the full stable eigenspace Y from H . However, computing Y is as expensive as solving a full-order LQR, with $\mathcal{O}(n^3)$ complexity for both computation and memory [30]. This may defeat the purpose of our design since we want our controller to be numerically much simpler to compute than the full-order LQR. To bypass this difficulty, we next show that Φ can be approximated by a matrix Φ_κ that follows from a κ -dimensional ($\kappa < n$, not necessarily equal to r) invariant subspace of Y . Ideally κ should be at most r to justify the computational benefit of our design while preserving an acceptable accuracy in the error norm ξ . This matrix Φ_κ is constructed as follows.

Definition V.2. Define $\Phi_\kappa \in \mathbb{R}^{n \times n}$ as

$$\Phi_\kappa := \Phi_\kappa^{\frac{1}{2}} \Phi_\kappa^{\frac{T}{2}} = Y_1(\Omega_1 B_d B_d^T \Omega_1^T \circ \mathcal{C}_{1,1})Y_1^T, \quad (27)$$

where $Y_1 = Y_{:,1:\kappa}$, $\Omega_1 = Y_{1:\kappa,:}^{-1}$ and $\mathcal{C}_{1,1} = \mathcal{C}_{1:\kappa,1:\kappa}$ are respectively the κ -dimensional partitions of Y , Y^{-1} and \mathcal{C} .

By definition of Φ_κ , one only needs to compute the first κ eigenvalues $\lambda_1^-, \dots, \lambda_\kappa^-$ of H , and the Y_1 component of the first κ eigenvectors. Ω_1 can be approximated by the pseudo-inverse of Y_1 . These κ smallest eigenvalues and eigenvectors can be solved by Krylov subspace-based techniques such as Arnoldi algorithm in $\mathcal{O}(n\kappa^2)$ time [30]. In addition, $\Phi_\kappa^{\frac{1}{2}} = Y_1(\Omega_1 B_d B_d^T \Omega_1^T \circ \mathcal{C}_{1,1})^{\frac{1}{2}}$ has a column dimension of κ . As a result, the complexity of Algorithm 1 is now reduced to $\mathcal{O}(n\kappa rk)$, where k is the total number of iterations. Therefore, the total complexity of Algorithm 1 followed by a reduced-order LQR design will be $\mathcal{O}(n\kappa^2) + \mathcal{O}(n\kappa rk) + \mathcal{O}(r^3)$, or at most $\mathcal{O}(nr^2 k)$ if $\kappa \leq r$, which is significantly more tractable compared to the $\mathcal{O}(n^3)$ complexity of full-order LQR, especially when r and κ are sufficiently small. The error in optimization for using $\Phi_\kappa^{\frac{1}{2}}$ instead of $\Phi^{\frac{1}{2}}$ as the input to Algorithm 1 can be quantified by the following lemma.

Lemma V.3. Assume Y^{-1} has a moderate condition number η , and each column of B_d has a unitary norm. The clustering matrix solved from the κ -dimensional approximation Φ_κ , namely $P_* = \arg\min_P \|(I_n - P^T P)\Phi_\kappa^{\frac{1}{2}}\|_F$, yields a worst-case error of

$$\begin{aligned} & \|(I_n - P_*^T P_*)\Phi^{\frac{1}{2}}\|_F - \|(I_n - P_*^T P_*)\Phi_\kappa^{\frac{1}{2}}\|_F \\ & \leq \sqrt{(n-r)\eta^2 n_b \sum_{i=\kappa+1}^n -\frac{1}{2\lambda_i^-}}. \end{aligned} \quad (28)$$

Proof. The proof is presented in the Appendix. \square

From Lemma V.3, Φ_κ will be most effective for k-means when the error $\sqrt{(n-r)\eta^2 n_b \sum_{i=\kappa+1}^n -\frac{1}{2\lambda_i^-}}$ is kept small. In practice, this situation happens when there exists κ ($\kappa \ll$

n) dominant eigenvalues in the Hamiltonian matrix, i.e., H exhibits a spectral gap as

$$0 > \lambda_1^- > \dots > \lambda_\kappa^- \gg \lambda_{\kappa+1}^- > \dots > \lambda_n^-.$$

This gap also occurs, for example, when the open-loop network has κ groups following coherency [3]. However, it is not necessary that the output of Algorithm 1 will be the same as these κ coherent groups. As a result of this spectral gap, we will have

$$\|\Phi_\kappa^{\frac{1}{2}}\|_F \gg \sqrt{(n-r)\eta^2 n_b \sum_{i=\kappa+1}^n -\frac{1}{2\lambda_i^-}}.$$

This inequality shows that by applying $\Phi_\kappa^{\frac{1}{2}}$ as the k-means input, the worst-case k-means error is negligible compared with the norm of $\Phi_\kappa^{\frac{1}{2}}$ itself. Therefore, Φ_κ will closely resemble Φ in solving the k-means optimization. The idea of utilizing a κ -dimensional subspace for computing Φ_κ is similar in spirit to finding an unstructured approximate ARE solution as proposed in [19]. However, it should be noted that the error bound in Lemma V.3 justifies the choice of the first κ eigenvectors for constructing Φ_κ in terms of reducing the approximation error, while the selection of the κ eigenvectors in [19] is undetermined.

VI. WEIGHT DESIGN FOR FIXED CLUSTERS

We next state a variant of our proposed controller where we minimize ξ by fixing the clustering set \mathcal{I} , and varying the projection weights in w instead. This type of controller may be needed when the physical nodes of the given network exhibit some kind of natural clustering based on their geographical distances from each other. In such situations, the operator of each cluster may prefer to have a dedicated coordinator for its own region instead of sharing a coordinator with nodes in other natural clusters. This scenario commonly arises in power system networks, where different parts of the grid are operated by different independent companies who prefer to maintain a certain degree of decentralization and privacy in sharing state information of their balancing regions with others. In Section VII we will see via simulations that the clusters assigned by Algorithm 1 are not guaranteed to intersect with these natural clusters. Therefore, in this section we develop a new algorithm where we fix \mathcal{I} to represent the natural clusters, and optimize ξ or $\|g_e(s)\|_{\mathcal{H}_2}$ over w . Note that the implementation architecture of the resulting controller is similar to the aggregate controller in [10], but the designs are very different since the controller in [10] is designed from singular perturbation-based models of the open-loop network. A visual interpretation of this approach and its comparison to the design in Section V are shown in Fig. 2. Note that the optimal values of w so obtained denote the relative *importance* of the network nodes in the closed-loop system with the projected controller. In Fig. 2c we show this relative importance by shrinking or expanding the size of the nodes. The size of a node should not be confused with its node-weight.

We consider the same optimization objective as in (19) but now minimize it with respect to w as

$$\underset{w}{\text{minimize}} \quad \xi = \|\Phi^{\frac{1}{2}} - P^T P \Phi^{\frac{1}{2}}\|_F. \quad (29)$$

To solve (29), we consider a binary projection matrix \hat{P} as

$$\hat{P}(i, j) := \begin{cases} 1 & j \in \mathcal{I}_i \\ 0 & \text{otherwise} \end{cases}.$$

As can be verified from Definition III.2, \hat{P} here also satisfies $P = \hat{P}\hat{W}$ with $\hat{W} = \text{diag}(\hat{w})$, where this \hat{w} is defined by

$$\hat{w}_j = \frac{w_j}{\|w_{\mathcal{I}_i}\|_2}, \quad j \in \mathcal{I}_i, \quad (30)$$

such that $\hat{w}_{\mathcal{I}_i}^T \hat{w}_{\mathcal{I}_i} = 1$, for $i = 1, \dots, r$. Using these notations, we can rewrite the objective function in (29) as

$$\begin{aligned} \xi^2 &= \text{tr}(\Phi - P^T P \Phi) = \text{tr}(\Phi) - \text{tr}(\hat{W} \hat{P}^T \hat{P} \hat{W} \Phi) \\ &= \text{tr}(\Phi) - \hat{w}^T (\hat{P}^T \hat{P} \circ \Phi) \hat{w}. \end{aligned}$$

Since $\text{tr}(\Phi)$ is a constant number, an equivalent form of (29) follows as

$$\begin{aligned} &\underset{\hat{w}}{\text{maximize}} \quad \hat{w}^T (\hat{P}^T \hat{P} \circ \Phi) \hat{w} \\ &\text{subject to} \quad \|\hat{w}_{\mathcal{I}_i}\|_2 = 1, \quad i = 1, \dots, r. \end{aligned} \quad (31)$$

The Hadamard product $\hat{P}^T \hat{P} \circ \Phi$ preserves the structure from $\hat{P}^T \hat{P}$, or equivalently from the clustering set \mathcal{I} in the objective function. As a result, the optimization problem (31) boils down to r decoupled optimizations

$$\begin{aligned} &\underset{\hat{w}_{\mathcal{I}_i}}{\text{maximize}} \quad \hat{w}_{\mathcal{I}_i}^T \Phi_{\mathcal{I}_i, \mathcal{I}_i} \hat{w}_{\mathcal{I}_i} \\ &\text{subject to} \quad \|\hat{w}_{\mathcal{I}_i}\|_2 = 1, \end{aligned} \quad (\text{opt1})$$

for $i = 1, \dots, r$, where $\Phi_{\mathcal{I}_i, \mathcal{I}_i}$ denotes the submatrix of Φ corresponding to the indices in \mathcal{I}_i . This decoupling can be illustrated by the same example we used before.

Example 3. (Continued) Consider the sets \mathcal{I}_1 , \mathcal{I}_2 and \mathcal{I}_3 , and the matrix

$$\hat{P} = \begin{bmatrix} 1 & 1 & 0 & 0 & 0 & 0 & 0 & 0 & 0 & 0 \\ 0 & 0 & 1 & 1 & 1 & 0 & 0 & 0 & 0 & 0 \\ 0 & 0 & 0 & 0 & 0 & 1 & 1 & 1 & 1 & 1 \end{bmatrix}.$$

The objective function in (31) can be block diagonalized as

$$\hat{w}^T (\hat{P}^T \hat{P} \circ \Phi) \hat{w} = \hat{w}^T \begin{bmatrix} \Phi_{1:2, 1:2} & 0 & 0 \\ 0 & \Phi_{3:5, 3:5} & 0 \\ 0 & 0 & \Phi_{6:10, 6:10} \end{bmatrix} \hat{w} = \begin{bmatrix} \hat{w}_{1:2}^T \Phi_{1:2, 1:2} \hat{w}_{1:2} & 0 & 0 \\ 0 & \hat{w}_{3:5}^T \Phi_{3:5, 3:5} \hat{w}_{3:5} & 0 \\ 0 & 0 & \hat{w}_{6:10}^T \Phi_{6:10, 6:10} \hat{w}_{6:10} \end{bmatrix}.$$

We next state the solution for (opt1) as follows.

Lemma VI.1. The global optimal for (opt1) is obtained at $\hat{w}_{\mathcal{I}_i} = \bar{v}(\Phi_{\mathcal{I}_i, \mathcal{I}_i})$, for $i = 1, \dots, r$.

Proof. Given $\hat{P}^T \hat{P} \succeq 0$ and $\Phi \succeq 0$, $\hat{P}^T \hat{P} \circ \Phi$ is positive-semidefinite according to the Schur product theorem. Also, the objective function in (opt1) is a standard Rayleigh quotient for symmetric eigenvalue problem. Therefore, the maximum

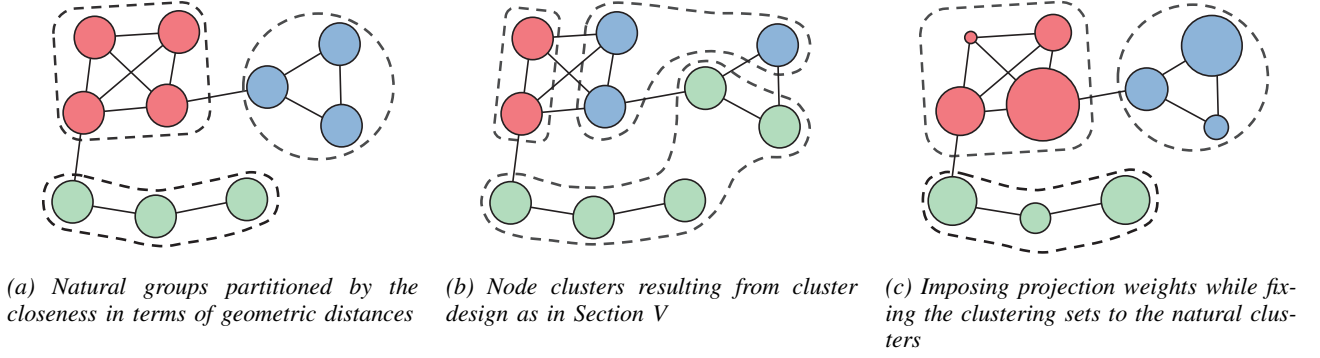


Figure 2: Illustration of cluster design and weight design.

value of objective function in (opt1) is obtained at the largest singular value of $\Phi_{\mathcal{I}_i, \mathcal{I}_i}$. Since $\Phi_{\mathcal{I}_i, \mathcal{I}_i} \succeq 0$, its largest singular value is the same as its largest eigenvalue $\bar{\lambda}(\Phi_{\mathcal{I}_i, \mathcal{I}_i})$, and hence the optimum is obtained at its dominant eigenvector $\bar{v}(\Phi_{\mathcal{I}_i, \mathcal{I}_i})$. \square

A. Co-Design for Satisfying Assumption IV.3

Once \hat{w} is solved from Lemma VI.1, one can choose any w that satisfies (30). However, such a solution merely guarantees the minimum for ξ in (29) at a fixed \mathcal{I} . Meanwhile, it is unclear whether γ , the upper bound for the \mathcal{H}_∞ norm in (16), would blow up due to the weight optimization. The worst case could be $w \perp \bar{v}$, which violates the crucial assumption about the stability of $\hat{g}(s)$, and as a result γ goes to infinity. Under this condition, there would be little validity in finding either the clustering sets or the weight from the bound (18). To avoid such a hazardous situation, we impose a supplementary design on (opt1) in order to move the first eigenvalue of $A - B\hat{K}$ away from 0. Recall that from (39) in the proof of Theorem V.1, one can derive the following equation

$$(A - G\hat{X})^T \hat{X} + \hat{X}(A - G\hat{X}) = (U^T U - P^T P)A^T \hat{X} + \hat{X}A(U^T U - P^T P) - 2P^T \tilde{Q}P.$$

In this form, by assuming v to be the eigenvector of $A - G\hat{X}$, the eigenvalue of $A - G\hat{X}$ can be represented by quadratic terms as

$$\lambda(A - G\hat{X}) = \frac{v^T(U^T U - P^T P)A^T \hat{X}v}{v^T \hat{X}v} - \frac{v^T P^T \tilde{Q}Pv}{v^T \hat{X}v},$$

where $v^T \hat{X}v > 0$ if $v \neq w$. Since $|v^T(U^T U - P^T P)A^T \hat{X}v| \leq 2\bar{\sigma}(A)\bar{\sigma}(\hat{X})$ is not sign-definite, a relaxation for minimizing the RHS would be to maximize the term $v^T P^T \tilde{Q}Pv$ with respect to w . However, finding a v that is the exact dominant eigenvector of $A - G\hat{X}$ is an intractable problem. Therefore, to conform to Assumption IV.3, we pose the co-design for (opt1) at $v = \bar{v}$ as

$$\begin{aligned} & \underset{\hat{w}}{\text{maximize}} && \bar{v}^T P^T \tilde{Q}P \bar{v} \\ & \text{subject to} && \|\hat{w}_{\mathcal{I}_i}\|_2 = 1, \quad i = 1, \dots, r. \end{aligned} \quad (\text{opt2})$$

Combining (opt2) with the main optimization (opt1) yields the final weight design problem as

$$\begin{aligned} & \underset{\hat{w}}{\text{maximize}} && [\hat{w}^T (\hat{P}^T \hat{P} \circ \Phi) \hat{w}]^2 + \rho \bar{v}^T P^T \tilde{Q}P \bar{v} \\ & \text{subject to} && \|\hat{w}_{\mathcal{I}_i}\|_2 = 1, \quad i = 1, \dots, r, \end{aligned} \quad (\text{opt3})$$

where $\rho > 0$ is a penalty factor. In (opt3), the objective function from (opt1) is squared to match with the order of the objective function in (opt2). This optimization problem is in the form of a fourth-order sum of squares (SOS) over $r > 1$ sphere constraints, for which finding even a local optimal is very difficult. One way to bypass this can be to approximate the second part of the objective function in (opt3) as $\rho \bar{v}^T (P^T \tilde{Q}P \circ \hat{P}^T \hat{P}) \bar{v}$, meaning that we approximate Q by retaining its block-diagonal components only. In this way, (opt3) is reduced to r SOS sub-problems with one sphere constraint for each as,

$$\begin{aligned} & \underset{\hat{w}}{\text{maximize}} && (\hat{w}_{\mathcal{I}_i} \otimes \hat{w}_{\mathcal{I}_i})^T (\Phi_{\mathcal{I}_i, \mathcal{I}_i} \otimes \Phi_{\mathcal{I}_i, \mathcal{I}_i} \\ & && + \rho Q_{\mathcal{I}_i, \mathcal{I}_i} \otimes \bar{v}_{\mathcal{I}_i} \bar{v}_{\mathcal{I}_i}^T) (\hat{w}_{\mathcal{I}_i} \otimes \hat{w}_{\mathcal{I}_i}) \\ & \text{subject to} && \|\hat{w}_{\mathcal{I}_i}\|_2 = 1, \end{aligned} \quad (\text{opt}^*)$$

for $i = 1, \dots, r$. While this approximation will follow naturally if Q is block-diagonal, the upshot is that the closed-loop performance of the projected system may suffer if Q has dominant off-block-diagonals. In practical networks, however, it is quite common to simply minimize the energy of a node itself, or the energy within a cluster, which implies that Q is very commonly a diagonal or block diagonal matrix. In fact, Q would indeed be preferred as block-diagonal for the scenario described in this section since network operators will always try to discourage closed-loop coupling of their own cluster nodes with other clusters. In those cases, (opt3) and (opt*) become equivalent problems, yielding the same solution. However, irrespective of whether Q is block-diagonal or not, the following theorem shows that the solution of (opt*) will satisfy Assumption IV.3.

Theorem VI.2. *Given the solutions $\hat{w}_{\mathcal{I}_i}$, $i = 1, \dots, r$ from (opt*) with $\rho > 0$, and sign normalization $\hat{w}_{\mathcal{I}_i} = \frac{\hat{w}_{\mathcal{I}_i}^T \bar{v}_{\mathcal{I}_i}}{|\hat{w}_{\mathcal{I}_i}^T \bar{v}_{\mathcal{I}_i}|} \hat{w}_{\mathcal{I}_i}$, $w \not\perp \bar{v}$ holds for any w satisfying (30).*

Proof. Note that the second part of the objective function in (opt*) can be rewritten as $\rho(\bar{v}_{\mathcal{I}_i}^T \hat{w}_{\mathcal{I}_i})^2 (\hat{w}_{\mathcal{I}_i}^T Q_{\mathcal{I}_i, \mathcal{I}_i} \hat{w}_{\mathcal{I}_i})$. Once

(opt*) is solved, each individual scalar $(\bar{v}_{\mathcal{I}_i}^T \hat{w}_{\mathcal{I}_i})^2$ has to be maximized away from 0, meaning $|\bar{v}_{\mathcal{I}_i}^T \hat{w}_{\mathcal{I}_i}| > 0$ for $i = 1, \dots, r$. Therefore, by the sign normalization shown above and (30), $w^T \bar{v} = \sum_{i=1}^r \|w_{\mathcal{I}_i}\| \|\bar{v}_{\mathcal{I}_i}^T \hat{w}_{\mathcal{I}_i}\| > 0$ is guaranteed for Assumption IV.3 to hold. \square

The following lemma shows the performance loss due to the approximation in (opt*) when Q is not block-diagonal.

Lemma VI.3. (Performance trade-off) *Let the maximum of (opt3) be J^{**} . The maximum J^* of (opt*) satisfies*

$$J^{**} - J_e \leq J^* \leq J^{**} + J_e, \quad (32)$$

where $J_e = \arg\max_{\substack{i=1,\dots,r \\ j,l=1,\dots,n}} \sum_{k=1}^r \rho |\bar{v}_l| \|Q_{\mathcal{I}_i(j), \mathcal{I}_k}\|_1 \|\bar{v}_{\mathcal{I}_k}\|_1$.

Proof. The proof follows directly from the Gershgorin circle theorem [30], and is shown in the Appendix. \square

B. Z-Eigenvalue Method for Solving (opt*)

Without loss of generality, we assume $\mathcal{I} = \{\mathcal{I}_1\}$, i.e., there is only one cluster in the network. This will allow us to drop the subscripts in all the variables used in (opt*), making the notations easier to follow. We define a fourth-order tensor $\mathcal{F} \in \mathbb{R}^{n \times n \times n \times n}$ as

$$\mathcal{F}_{i,j,k,l} = \Phi_{i,j} \Phi_{k,l} + \rho Q_{i,j} \bar{v}_k \bar{v}_l, \quad i, j, k, l = 1, \dots, n. \quad (33)$$

After a few manipulations, it can be shown that (opt*) is equivalent to the following problem

$$\begin{aligned} & \underset{\hat{w}}{\text{maximize}} && \mathcal{F} \odot (\hat{w} \otimes \hat{w} \otimes \hat{w} \otimes \hat{w}) \\ & \text{subject to} && \|\hat{w}\|_2 = 1, \end{aligned} \quad (\text{opt**})$$

where \odot denotes the element-wise product. It has been studied in [15] that such a polynomial optimization is equivalent to finding the largest Z -eigenvalue of \mathcal{F} , if \mathcal{F} is super-symmetric. From the definition in [15], a super-symmetric tensor is one whose entries are invariant to any permutation to the index, i.e. $\mathcal{F}_{i,j,k,l} = \dots = \mathcal{F}_{l,k,j,i}$, which fails for (33) as $\mathcal{F}_{i,j,k,l} \neq \mathcal{F}_{i,k,j,l}$. However, note that although \mathcal{F} is not super symmetric, $\mathcal{F} \odot (\hat{w} \otimes \hat{w} \otimes \hat{w} \otimes \hat{w})$ is a one-dimensional polynomial which is invariant to any index permutations.³ Following this logic, we rewrite the objective function in (opt**) as follows.

Proposition VI.4. *Given the fourth-order tensor \mathcal{F} specified by (33), the polynomial $\mathcal{F} \odot (\hat{w} \otimes \hat{w} \otimes \hat{w} \otimes \hat{w})$ is identical to*

$$\mathcal{F}^s \odot (\hat{w} \otimes \hat{w} \otimes \hat{w} \otimes \hat{w}) = (\hat{w} \otimes \hat{w})^T \mathcal{F}^s (\hat{w} \otimes \hat{w}),$$

where \mathcal{F}^s is a super-symmetric tensor specified by

$$\begin{aligned} \mathcal{F}_{i,j,k,l}^s &= \frac{1}{3}(\Phi_{i,j} \Phi_{k,l} + \Phi_{i,k} \Phi_{j,l} + \Phi_{i,l} \Phi_{j,k}) + \frac{1}{6} \rho (Q_{i,j} \bar{v}_k \bar{v}_l \\ &+ Q_{i,k} \bar{v}_j \bar{v}_l + Q_{i,l} \bar{v}_j \bar{v}_k + Q_{j,k} \bar{v}_i \bar{v}_l + Q_{j,l} \bar{v}_i \bar{v}_k + Q_{k,l} \bar{v}_i \bar{v}_j) \end{aligned}$$

for $i, j, k, l = 1, \dots, n$, and $\mathcal{F}^s \in \mathbb{R}^{n^2 \times n^2}$, the matrix unfolding of \mathcal{F}^s , can be obtained from

$$F_{n(i-1)+k, n(j-1)+l}^s = \mathcal{F}_{i,j,k,l}^s, \quad i, j, k, l = 1, \dots, n.$$

³This is analogous to an unsymmetric matrix whose quadratic form is invariant to the transpose operation, i.e. $z^T \frac{F^T + F}{2} z = z^T F z = z^T F^T z \in \mathbb{R}$.

The proof is omitted as the equations above can be easily verified by matching the coefficients of the polynomials on both sides.

In summary, the optimization problem (opt**) can be approached by substituting \mathcal{F} with a super-symmetric tensor \mathcal{F}^s . One can, thereafter, solve (opt**) using techniques developed for Z -eigenvalue problems. We solve (opt**) using the tensor power iteration method [33] in Algorithm 2. The convergence properties of this algorithm can be found in [33]. Due to the super symmetry of \mathcal{F}^s , the worst case (only one cluster) complexity for each iteration of Algorithm 2 is $\mathcal{O}(n^4/4)$. Although this computation cost is expensive, the algorithm can be easily parallelized, and is easier to implement than $\mathcal{O}(n^3)$ full-order LQR as the memory required is only $\mathcal{O}(n^2)$. Moreover, the value of n for Algorithm 2 scales down as the number of clusters increases.

Algorithm 2: Power iteration for projection weight design

Input : Φ (or Φ_κ), Q , \bar{v} , \mathcal{I} , ρ and δ

- 1 Partition $\Phi_{\mathcal{I}_i, \mathcal{I}_i}$, $Q_{\mathcal{I}_i, \mathcal{I}_i}$ and $\bar{v}_{\mathcal{I}_i}$ based on \mathcal{I} ;
- 2 **for** $i = 1, \dots, r$ **do**
- 3 Find F^s corresponding to \mathcal{I}_i by Proposition VI.4;
- 4 **Initialization:** Compute the dominant eigenvector of F^s as $\bar{v}(F^s)$, then choose the initial vector v^0 as $v^0 = \bar{v}(\text{unvec}(\bar{v}(F^s)))$;
- 5 $k = 1$;
- 6 **while** $\frac{(v^k \otimes v^k)^T F^s (v^k \otimes v^k)}{(v^{k-1} \otimes v^{k-1})^T F^s (v^{k-1} \otimes v^{k-1})} - 1 > \delta$ **or within maximum iterations do**
- 7 $v^k = \text{unvec}(F^s(v^{k-1} \otimes v^{k-1}))v^{k-1}$;
- 8 $v^k = \frac{v^k}{\|v^k\|_2}$;
- 9 $k = k + 1$;
- 10 **end**
- 11 $\hat{w}_{\mathcal{I}_i} = v^k$;
- 12 **end**
- 13 Construct w and then P by (30);

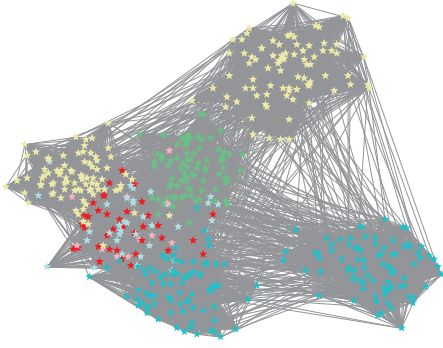
Output: P

C. Optimizing ξ with respect to both \mathcal{I} and w

The designs proposed in Section V and VI can be combined to optimize ξ as a function of both \mathcal{I} and w iteratively. In this case, one would start with an arbitrarily chosen w , and minimize ξ with respect to \mathcal{I} using Algorithm 1. Say, the optimal cluster set is given as \mathcal{I}^* . Thereafter, one would fix \mathcal{I} to \mathcal{I}^* , and minimize ξ with respect to w using Algorithm 2, and so on. The resulting algorithm is shown in Algorithm 3.

VII. NUMERICAL EXAMPLES

To verify our proposed algorithms, we use a network model defined over a 500-node graph \mathcal{G}_{500} . The graph is randomly generated with 0.5 overall probability for edge attachment, and 6 natural clusters with a proportion of 100 for the number of edges within clusters versus the number of edges across clusters. This setting yields the worst-case singular



(a) Clusters by coherency clustering

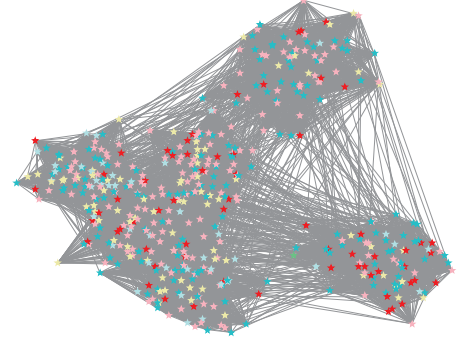
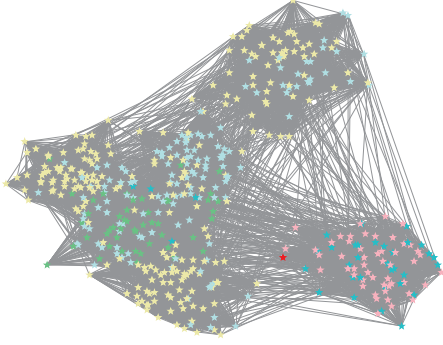
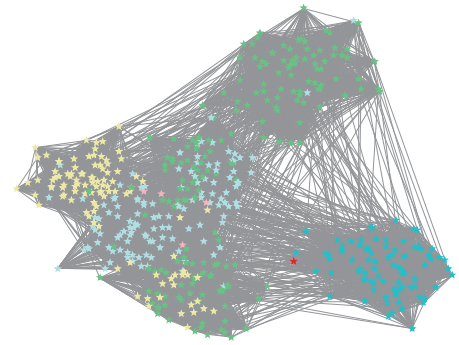
(b) Clusters by \mathcal{H}_2 open-loop clustering(c) Clusters by \mathcal{H}_2 closed-loop clustering with Q_1 (d) Clusters by \mathcal{H}_2 closed-loop clustering with Q_2

Figure 3: Clustering of the 500-node network with $r = 6$ clusters. Nodes assigned to the same cluster are marked by the same color in one figure. Note that only the node identities are comparable between figures, but not the cluster identities.

Algorithm 3: Iterative algorithm for finding P

Input : A, B, B_d, Q, R and r

- 1 Compute $\Phi_{\kappa}^{\frac{1}{2}}$ by Definition V.2;
- 2 Choose $w^0 = \bar{v}$, and compute $W^0 = \text{diag}(w^0)$ and the k-means input $\Psi^0 = (W^0)^{-1}\Phi_{\kappa}^{\frac{1}{2}}$;
- 3 $k = 1$;
- 4 **while** $\mathcal{I}^{k-1} \neq \mathcal{I}^k$ or within maximum iterations **do**
- 5 Solve \mathcal{I}^k from Algorithm 1 by (Ψ^{k-1}, w^{k-1}, r) ;
- 6 Update w^k from Algorithm 2 by \mathcal{I}^k ;
- 7 $k = k + 1$;
- 8 **end**

Output: P

perturbation parameter δ [3] to be at most 0.01 for \mathcal{G}_{500} . We also apply a random weight $1 \leq M_{i,i} \leq 2$ on each node. The disturbance is assumed to enter from the 364th node, i.e. B_d equals to the 364th column of I_{500} . We assume $B = R = I_{500}$ and two choices of Q as: a scaled identity matrix $Q_1 = 1000 \times I_{500}$, and $Q_2 = [L(\mathcal{G}_{500})]^2$, which is the square of the unweighted Laplacian matrix of \mathcal{G}_{500} . Both Q_1 and Q_2 satisfy the solvability condition in Theorem IV.2 and the stability condition in Theorem IV.5.

A. Cluster Design

We start by finding the closed-loop clustering set \mathcal{I} with respect to a fixed weight $w = \bar{v}$ with $r = 6$. For comparison,

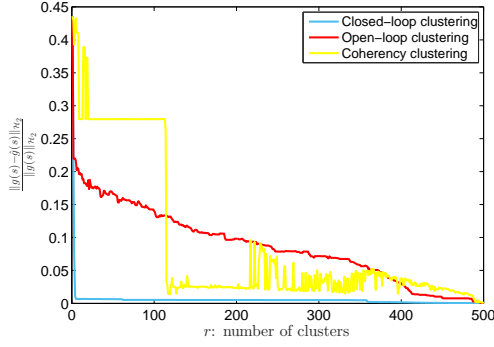
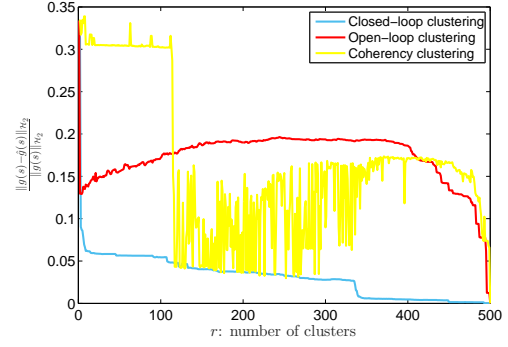
Table I: Input specifications for Algorithm 1

| Algorithm | Data | Weight | Number of Clusters |
|---|------------|----------------|--------------------|
| \mathcal{H}_2 closed-loop clustering | Φ | w | r |
| \mathcal{H}_2 open-loop clustering [18] | Φ_o^a | w | r |
| Coherency clustering [3] | Φ_c^b | $\mathbf{1}_n$ | r |

^a Let v_c^T be the complement of \bar{v}^T , and then $\Phi_o := \Phi_o^{\frac{1}{2}} \Phi_o^{\frac{T}{2}} = v_c [\int_0^\infty e^{(v_c^T A v_c) \tau} v_c^T B_d B_d^T v_c e^{(v_c^T A^T v_c) \tau} d\tau] v_c^T$.

^b Let the eigenvalues of $-L_m(\mathcal{G})$ be $0 = \lambda_1 > \lambda_2 \geq \dots \geq \lambda_n$, $\Psi_c = [v_1, \dots, v_r]$ where v_i is the right eigenvector of λ_i .

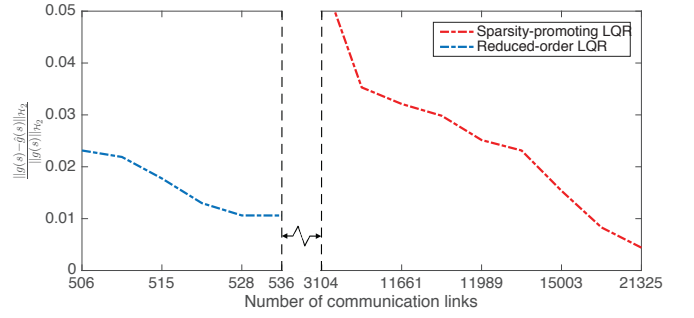
we also apply two other popular clustering algorithms, namely, \mathcal{H}_2 open-loop clustering proposed in [18], and coherency-based clustering proposed in [3]. Both of these clustering algorithms can be transformed into Algorithm 1, with their equivalent inputs as summarized in Table I. Note that these two algorithms capture only the open-loop characteristics of the network, and hence do not depend on the choice of Q and R . Fig. 3a shows that the clusters identified by coherency based clustering closely resemble the natural clusters of the open-loop network except for a few discrepancies. For example, two distant groups of nodes are assigned to the same cluster shown in yellow. These discrepancies arise from the fact that the natural clusters are only based on the edge-weights (that model geographical distance between two nodes), while coherent clusters are decided by both edge-weights and node-weights. The \mathcal{H}_2 open-loop clusters are shown in Fig. 3b. As such, they do not follow any definite pattern with respect to the natural clusters as they are based on node aggregation following from

(a) Design with Q_1 (b) Design with Q_2 Figure 4: Performance loss $\frac{\|g(s) - \hat{g}(s)\|_{\mathcal{H}_2}}{\|g(s)\|_{\mathcal{H}_2}}$ with respect to the number of clusters

the \mathcal{H}_2 -norm distance of their output responses. Figures 3c and 3d, on the other hand, show the clusters identified by our \mathcal{H}_2 closed-loop algorithm (Algorithm 1) for $Q = Q_1$ and $Q = Q_2$, respectively. Both of these clusters are different from each other for obvious reasons. They are also different from the natural clusters, the coherent clusters as well as the \mathcal{H}_2 open-loop clusters as Algorithm 1 is related to the closed-loop controllability subspace.

We also illustrate the effectiveness of \mathcal{H}_2 closed-loop clustering with respect to the number of clusters r . As evident from the design, the error between the transfer matrices in (5) and (10) will be minimal when $r = n$, and will degrade with decreasing r while improving tractability of the design. We vary r from 1 to 500, and calculate the ratio $\frac{\|g(s) - \hat{g}(s)\|_{\mathcal{H}_2}}{\|g(s)\|_{\mathcal{H}_2}}$ resulting from the three clustering algorithms. The results are shown in Fig. 4. For both Q_1 and Q_2 the closed-loop clustering outperforms the other two methods in approaching the \mathcal{H}_2 performance of $g(s)$. Therefore, even for very small values of r , the projected controller achieves significantly close \mathcal{H}_2 performance as the full-order LQR controller. In terms of implementation, the projected controller needs far less number of communication links than a full-order standard LQR as well as a full-order \mathcal{L}_1 sparsity-promoting LQR [16]. For example, for this system a standard LQR would require $\binom{500}{2} = 124750$ links. Meanwhile as shown in Fig. 5, a sparsity promoting LQR requires from 3104 to as many as 21325 links to retain a performance loss under 5%. By choosing $r \leq 9$, the similar performance loss can be maintained by our design using at most 536 links.

It is also noted that the \mathcal{H}_2 closed-loop clusters do not need to strictly follow the natural geometric clustering of the network. For example, in both Figures (3c) and (3d), a cluster can be one single node as shown by the red, or can be scattered over the network such as yellow. In practice, this means that to implement the proposed control law, nodes from different geographical locations may need to be part of the same cluster for the closed-loop model, i.e., nodes that belong to two different natural clusters in open-loop may need to collaborate and send their states to a common coordinator. The assignment, therefore, encourages system-wide participation from nodes at various corners of \mathcal{G}_{500} for implementing the

Figure 5: Projected LQR controller from clustering vs. LQR controller from sparsity-promoting algorithm with Q_1 .

controller.

B. Weight Design

We next apply Algorithm 2 on \mathcal{G}_{500} to find the optimal projection weight w while fixing the clusters to those obtained from coherency. These clusters as previously shown in Fig. 3a closely resemble the natural clusters, and their clustering sets are given by $\mathcal{I}_1 = \{1, \dots, 167\}$, $\mathcal{I}_2 = \{168, \dots, 178\}$, $\mathcal{I}_3 = \{179, \dots, 344\}$, $\mathcal{I}_4 = \{345, \dots, 379\}$, $\mathcal{I}_5 = \{380, \dots, 463\}$ and $\mathcal{I}_6 = \{464, \dots, 500\}$. After running the algorithm with both Q_1 and Q_2 , we plot the two weight vectors compared with \bar{v} in Fig. 6. It can be seen that the weight vectors from Q_1 and Q_2 are very different than \bar{v} or between themselves. On the other hand, both of these weights at the 364th node, i.e., the node where the disturbance enters, show a sudden jump in magnitude from the rest of the nodes. To verify the closed-loop performance, we construct the P matrices using these two vectors, and summarize the error ratios with some design parameters in Table II. As expected, by applying the weight design, the closed-loop errors as shown in Table II are significantly reduced from $w = \bar{v}$. Despite the fact that these two errors are much larger than what we get from closed-loop clustering (which yields an error of 0.68%), the weight design still grants us with significant improvement over the hard constraint on \mathcal{I} .

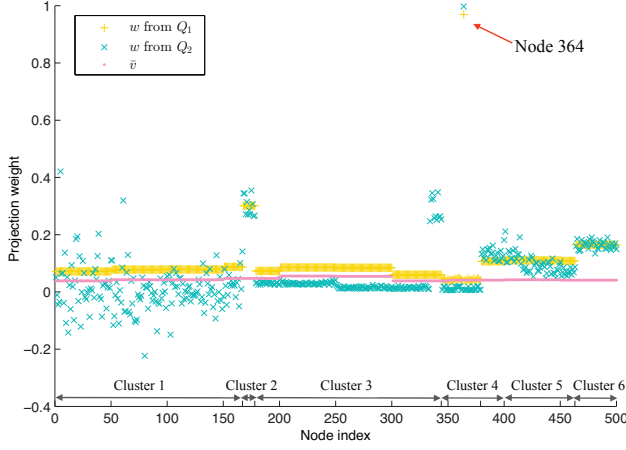
Finally, we compare the closed-loop performance of the iterative Algorithm 3 (where both w and \mathcal{I} are free) with

Table II: Results of weight design

| Case | Penalty factor ρ | Relative error $\ g(s) - \hat{g}(s)\ _{\mathcal{H}_2} / \ g(s)\ _{\mathcal{H}_2}$ | |
|-------|--|---|---------------------------|
| | | with $w = \bar{v}$ | with w from Algorithm 2 |
| Q_1 | $0.011 \frac{\ \Phi\ _2}{\bar{v}^T Q \bar{v}}$ | 29.14% | 7.35% |
| Q_2 | $0.007 \frac{\ \Phi\ _2}{\bar{v}^T Q \bar{v}}$ | 35.69% | 21.79% |

¹ The convergence threshold for power iteration is chosen as $\delta = 0.05$.

² $\frac{\|\Phi\|_2}{\bar{v}^T Q \bar{v}}$ is included in the penalty factor to normalize the two objective functions in (opt*) to the same scale.

Figure 6: Weight designs from Q_1 and Q_2

Algorithm 1 in Fig. 7. The comparison is shown for Q_1 and only $r \leq 6$ as the error ratio already becomes under 1% after $r = 6$. For this example, it is worth mentioning that Algorithm 3 turns out to be surprisingly efficient as it converges right after the first iteration. In this sense, the iterative process reduces to a single weight design after the clustering. Fig. 7 testifies that Algorithm 3 achieves better matching between $g(s)$ and $\hat{g}(s)$ than Algorithm 1.

C. Scalability Results

To verify the scalability of Algorithm 1, we increase the size of the network, and compare the computation time with that of solving a full-order LQR controller. We let $r = 5$ and $\kappa = 5$ for computing $\Phi_{\kappa}^{\frac{1}{2}}$, and present the results in Table III. The table verifies the $\mathcal{O}(n^3)$ complexity for full-order LQR vs. the $\mathcal{O}(nr^2k)$ complexity for reduced-order LQR, where k is the number of iterations. When $n = 8000$, the full-order LQR is

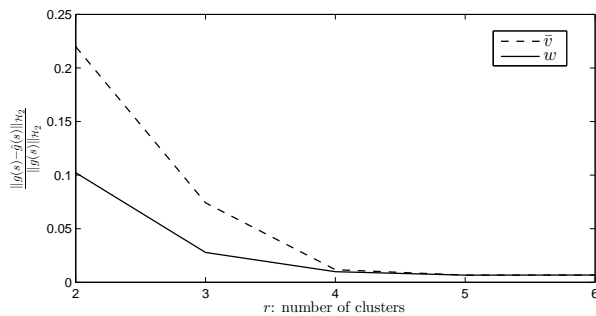


Figure 7: Performance loss by weight refinement

Table III: Scalability Results

| n | Computation time | | Perf. loss $\frac{\ g(s) - \hat{g}(s)\ _{\mathcal{H}_2}}{\ g(s)\ _{\mathcal{H}_2}}$ |
|-------|------------------|---------------|---|
| | Full-order | Reduced-order | |
| 1000 | 16.34 sec | 0.79 sec | 3.74% |
| 2000 | 134.91 sec | 2.64 sec | 1.06% |
| 4000 | 20.36 min | 11.61 sec | 0.25% |
| 6000 | 71.06 min | 24.73 sec | 0.13% |
| 8000 | Out of memory | 48.39 sec | - |
| 10000 | Out of memory | 75.90 sec | - |

already beyond the capability of our computation facility. The reduced-order LQR design, however, requires remarkably less computation time, while still providing a close performance match to the full-order LQR controller.

VIII. CONCLUSION

In this paper we developed a set of projection-based algorithms that improve the dynamic response of large consensus networks with reduced-order LQR controllers. The advantage of these reduced-order controllers is that they are structured, and significantly easier to design and implement compared to regular full-order LQR controllers. Our future work will be to address the robustness of this approach to communication delays, to exploit additional input-output properties of consensus networks such as passivity to further improve performance, and to inspect the influence of network heterogeneity on clustering.

APPENDIX: PROOFS

The following result from [29] will be used in proving Lemma IV.7 and Theorem V.1.

Lemma 1.5 in [29]: The solution X from the ARE (4) has the following upper bound on its maximal eigenvalue:

$$\bar{\lambda}(X) \leq \bar{\lambda}(D_t^T D_t) \frac{\bar{\lambda}[(Q + K_t^T K_t) D_t^T D_t]}{\underline{\lambda}(F D_t^T D_t)}, \quad (34)$$

where K_t is any matrix stabilizing $A + BR^{-\frac{1}{2}}K_t$, and the non-singular matrix D_t and positive-definite matrix $F = F^T$ are chosen such that $(A + BR^{-\frac{1}{2}}K_t)^T D_t^T D_t + D_t^T D_t (A + BR^{-\frac{1}{2}}K_t) \leq -F$.

A. Proof of Lemma IV.7

By letting $K_t = -R^{-\frac{T}{2}}B^T$, $D_t = I_n$ and $F = 2G - 2A > 0$ in (34), an upper bound for $\bar{\sigma}(X) = \bar{\lambda}(X)$ can be found by $\bar{\lambda}(X) \leq \frac{\bar{\sigma}(Q+G)}{2\underline{\sigma}(G-A)} = \beta$. Note that (12) is satisfied if

$$\underline{\sigma}(Q) > 2\bar{\sigma}(X)\bar{\sigma}(G)\bar{\sigma}(E), \quad (35)$$

where the RHS is further bounded by

$$2\bar{\sigma}(X)\bar{\sigma}(G)\bar{\sigma}(E) \leq 2\beta\bar{\sigma}(G)[\beta + \bar{\sigma}(\hat{X})]. \quad (36)$$

Therefore, (35), and then (12) will hold if $\underline{\sigma}(Q)$ is greater than the RHS of (36), which yields (13) in Lemma IV.7.

B. Proof of Theorem V.1

We divide the proof into three steps.

1) : We derive an analytic expression for E by recovering the reduced-order ARE as shown in (9) to the full dimension as

$$P^T(\tilde{A}^T \tilde{X} + \tilde{X} \tilde{A} + \tilde{Q} - \tilde{X} \tilde{G} \tilde{X})P = 0. \quad (37)$$

Notice that A and \tilde{A} are related by

$$\tilde{A}P = PA - PAU^T U, \quad (38)$$

where U is the complement of P as noted before. Thereby substituting $\tilde{A}P$ and $P^T \tilde{A}^T$ in terms of (38), and after a few calculations, (37) yields the approximated ARE (for details, please see [32])

$$A^T \hat{X} + \hat{X} A + Q - \hat{X} G \hat{X} = \mathcal{R}, \quad (39)$$

with

$$\mathcal{R} := U^T U A^T \hat{X} + \hat{X} A U^T U + Q - P^T \tilde{Q} P \quad (40)$$

denoting the residue of the approximate ARE. It can be easily verified that \mathcal{R} satisfies the Galerkin condition, i.e. $P \mathcal{R} P^T = 0$. By subtracting (4) from (39), we get the following Sylvester equation

$$(A - G\hat{X})^T E + E(A - GX) = -\mathcal{R}. \quad (41)$$

From (41), we are able to explicitly write E as a function of $A - GX$, $A - G\hat{X}$ and \mathcal{R} , and hence obtain an initial bound for $\|E\Phi^{\frac{1}{2}}\|_F$ in the next step.

2) : Pre- and post-multiplying (41) with $\Phi^{\frac{T}{2}}$ and $\Phi^{\frac{1}{2}}$ respectively, the Sylvester equation takes the form

$$\mathcal{A}\Phi^{\frac{T}{2}}E\Phi^{\frac{1}{2}} + \Phi^{\frac{T}{2}}E\Phi^{\frac{1}{2}}\mathcal{B} = -\Phi^{\frac{T}{2}}\mathcal{R}\Phi^{\frac{1}{2}}, \quad (42)$$

where we use the notations $\mathcal{A} = \Phi^{\frac{T}{2}}(A - G\hat{X})^T \Phi^{-\frac{T}{2}}$ and $\mathcal{B} = \Phi^{-\frac{1}{2}}(A - GX)\Phi^{\frac{1}{2}}$ for brevity. It can be easily shown that $\lambda(\mathcal{A}) < 0$ and $\lambda(\mathcal{B}) < 0$, which implies $\lambda_i(\mathcal{A}) + \lambda_j(\mathcal{B}) \neq 0$ for any $i, j = 1, \dots, n$ so that (42) is solvable. From Equation (42), $\mathcal{L}_{\mathcal{A}, \mathcal{B}}^{-1}(\cdot)$, the inverse Sylvester operator with respect to \mathcal{A} and \mathcal{B} , is specified by

$$\mathcal{L}_{\mathcal{A}, \mathcal{B}}^{-1}(-\Phi^{\frac{T}{2}}\mathcal{R}\Phi^{\frac{1}{2}}) = \text{unvec}[\mathcal{L}^{-1} \cdot \text{vec}(-\Phi^{\frac{T}{2}}\mathcal{R}\Phi^{\frac{1}{2}})], \quad (43)$$

where $\mathcal{L}^{-1} = (I_n \otimes \mathcal{A} + \mathcal{B} \otimes I_n)^{-1}$ is an $n^2 \times n^2$ matrix. Therefore, the weighted error $E\Phi^{\frac{1}{2}}$ can be expressed as

$$E\Phi^{\frac{1}{2}} = \Phi^{-\frac{T}{2}} \cdot \mathcal{L}_{\mathcal{A}, \mathcal{B}}^{-1}(-\Phi^{\frac{T}{2}}\mathcal{R}\Phi^{\frac{1}{2}}). \quad (44)$$

Since the Frobenius norm is unitary invariant (invariant to the change of basis), taking norm on both sides of (44) provides an upper bound on $\|E\Phi^{\frac{1}{2}}\|_F$ as

$$\|E\Phi^{\frac{1}{2}}\|_F \leq \|\Phi^{-\frac{1}{2}}\|_F \|\mathcal{L}^{-1}\|_F \|\Phi^{\frac{T}{2}}\mathcal{R}\Phi^{\frac{1}{2}}\|_F. \quad (45)$$

Note that $\|\mathcal{L}^{-1}\|_F$ satisfies $\|\mathcal{L}^{-1}\|_F \leq \sqrt{n^2 \bar{\sigma}(\mathcal{L}^{-1})} = \frac{n}{\underline{\sigma}(\mathcal{L})}$, where $\underline{\sigma}(\mathcal{L})$ is calculated by $\underline{\sigma}^2(\mathcal{L}) = \underline{\lambda}(\mathcal{L}\mathcal{L}^T)$ with

$$\mathcal{L}\mathcal{L}^T = I_n \otimes \mathcal{A}\mathcal{A}^T + \mathcal{B}\mathcal{B}^T \otimes I_n + \mathcal{B}^T \otimes \mathcal{A} + \mathcal{B} \otimes \mathcal{A}^T.$$

The eigenvalues of $\mathcal{B}^T \otimes \mathcal{A}$ are counted by $\lambda_i(\mathcal{A})\lambda_j(\mathcal{B})$ with $i, j = 1, \dots, n$, and according to the Weyl's inequality of eigenvalues [28], we have the lower bound for $\underline{\sigma}^2(\mathcal{L})$ as

$$\begin{aligned} \underline{\sigma}^2(\mathcal{L}) &\geq \underline{\lambda}(\mathcal{A}\mathcal{A}^T) + \underline{\lambda}(\mathcal{B}\mathcal{B}^T) + 2\underline{\lambda}(\mathcal{B}^T \otimes \mathcal{A}) \\ &= \underline{\sigma}^2(\mathcal{A}) + \underline{\sigma}^2(\mathcal{B}) + 2\underline{\lambda}(\mathcal{A})\underline{\lambda}(\mathcal{B}) \geq \underline{\sigma}^2(\mathcal{B}). \end{aligned} \quad (46)$$

Combining (45) with (46) then yields the following bound⁴

$$\|E\Phi^{\frac{1}{2}}\|_F \leq \epsilon_1 n \|\Phi^{\frac{T}{2}}\mathcal{R}\Phi^{\frac{1}{2}}\|_F, \quad (47)$$

where $\epsilon_1 = \frac{\|\Phi^{-\frac{1}{2}}\|_F}{\underline{\sigma}[\Phi^{-\frac{1}{2}}(A - GX)\Phi^{\frac{1}{2}}]} > 0$ is independent of P . However, in (47) the norm of the weighted residue $\Phi^{\frac{T}{2}}\mathcal{R}\Phi^{\frac{1}{2}}$, as written by

$$\begin{aligned} \Phi^{\frac{T}{2}}\mathcal{R}\Phi^{\frac{1}{2}} &= \Phi^{\frac{T}{2}}U^T U A^T \hat{X} \Phi^{\frac{1}{2}} + \Phi^{\frac{T}{2}}\hat{X} A U^T U \Phi^{\frac{1}{2}} \\ &+ \Phi^{\frac{T}{2}}(Q U^T U + U^T U Q - U^T U Q U^T U) \Phi^{\frac{1}{2}}, \end{aligned} \quad (48)$$

contains the inexplicit functional \hat{X} . We then bypass this term in the final step.

3) : Taking norm on both sides of (48), and then isolating the norm of \hat{X} , we can form the bound

$$\|\Phi^{\frac{T}{2}}\mathcal{R}\Phi^{\frac{1}{2}}\|_F \leq 2\xi(\|A\|_F \|\Phi^{\frac{1}{2}}\|_F \|\hat{X}\|_F + \|Q\Phi^{\frac{1}{2}}\|_F) + \xi^2 \|Q\|_F, \quad (49)$$

with $\xi = \|U^T U \Phi^{\frac{1}{2}}\|_F$. Recall that $\|\hat{X}\|_F = \|P^T \tilde{X} P\|_F = \|\tilde{X}\|_F$, where \tilde{X} is the solution of the reduced-order ARE (9). Applying (34) in (9), and choosing $K_t = -\tilde{R}^{-\frac{T}{2}} \tilde{B}$, $D_t = I_r$ and $F = 2\tilde{G} - 2\tilde{A} \succ 0$, $\|\tilde{X}\|_F$ satisfies

$$\|\tilde{X}\|_F \leq \sqrt{r\bar{\sigma}(\tilde{X})} \leq \frac{\sqrt{r\bar{\sigma}(\tilde{Q} + \tilde{G})}}{2\underline{\sigma}(\tilde{G} - \tilde{A})} \leq \frac{\sqrt{r\bar{\sigma}(Q + G)}}{2\underline{\sigma}(G - A)}, \quad (50)$$

where the last bound is made by eigenvalue interlacing property of symmetric matrix [28]. The Theorem V.1 follows from (47), (49) and (50).

C. Proof of Lemma V.3

To prove the error bound (28), we define a matrix $\bar{\Phi}$ as

$$\bar{\Phi} = [\bar{\Phi}_1 \quad \dots \quad \bar{\Phi}_{n_b}], \quad (51)$$

where $\bar{\Phi}_i = Y \text{diag}(Y^{-1} b_i) \mathcal{C}_{\frac{1}{2}}^{\frac{1}{2}}$, $i = 1, \dots, n_b$ and b_i is the i^{th} column of B_d . Since the matrix $\bar{\Phi}$ satisfies $\bar{\Phi} = \bar{\Phi} \bar{\Phi}^T = \Phi^{\frac{1}{2}} \Phi^{\frac{T}{2}}$, it can be easily verified that $\|\bar{\Phi}_{i,:} - \bar{\Phi}_{j,:}\|_2 = \|\Phi_{i,:}^{\frac{1}{2}} - \Phi_{j,:}^{\frac{1}{2}}\|_2$ for $i, j = 1, \dots, n$. This means that when applied as the inputs to the k-means, $\bar{\Phi}$ and $\Phi^{\frac{1}{2}}$ yield the same distance measure, and thus the same clustering results. Therefore, we can use the equivalent matrix $\bar{\Phi}$ to derive the analysis afterwards. Besides Y_1 and Ω_1 defined in Definition V.2, we further denote $Y_2 = Y_{:, \kappa+1, n}$ and $\Omega_2 = Y_{\kappa+1, :, n}^{-1}$, and partition the Cholesky Decomposition $\mathcal{C}_{\frac{1}{2}}^{\frac{1}{2}}$ as

$$\mathcal{C}_{\frac{1}{2}}^{\frac{1}{2}} = \begin{bmatrix} \mathcal{C}_{1,1}^{\frac{1}{2}} & 0 \\ \mathcal{C}_{2,1}^{\frac{1}{2}} & \mathcal{C}_{2,2}^{\frac{1}{2}} \end{bmatrix} = \begin{bmatrix} \mathcal{C}_{1:\kappa, 1:\kappa}^{\frac{1}{2}} & 0 \\ \mathcal{C}_{\kappa+1:n, 1:\kappa}^{\frac{1}{2}} & \mathcal{C}_{\kappa+1:n, \kappa+1:n}^{\frac{1}{2}} \end{bmatrix}.$$

With these notations, $\bar{\Phi}_i$ in (51) can be decomposed into $\bar{\Phi}_i = \bar{\Phi}_{i,s} + \bar{\Phi}_{i,f}$, where $\bar{\Phi}_{i,s} = [Y_1 \text{diag}(\Omega_1 b_i) \mathcal{C}_{1,1}^{\frac{1}{2}} \quad 0]$ and $\bar{\Phi}_{i,f} = [Y_2 \text{diag}(\Omega_2 b_i) \mathcal{C}_{2,1}^{\frac{1}{2}} \quad Y_2 \text{diag}(\Omega_2 b_i) \mathcal{C}_{2,2}^{\frac{1}{2}}]$, and thus Φ_{κ} can be rewritten as $\Phi_{\kappa} = \sum_{i=1}^{n_b} \bar{\Phi}_{i,s} \bar{\Phi}_{i,s}^T$. Notice that $\xi = \|(I_n - P^T P) \Phi^{\frac{1}{2}}\|_F = \|(I_n - P^T P) \bar{\Phi}\|_F$ satisfies

$$\xi \leq \|(I_n - P^T P) \Phi_{\kappa}^{\frac{1}{2}}\|_F + \|(I_n - P^T P) \bar{\Phi}_f\|_F, \quad (52)$$

⁴In general, Weyl's inequality does not guarantee tightness of bounds for eigenvalues that lie in between the minimum and maximum eigenvalues. The bound on maximum eigenvalues in (46), however, is relatively tighter.

where $\bar{\Phi}_f = [\bar{\Phi}_{1,f} \ \cdots \ \bar{\Phi}_{n_b,f}]$. The second norm on the RHS of (52) is further bounded by

$$\begin{aligned} \|(I_n - P^T P)\bar{\Phi}_f\|_F &\leq \sqrt{(n-r)}\|\bar{\Phi}_f\|_F \\ &\leq \sqrt{(n-r)\eta^2 \sum_{i=1}^{n_b} (\|\mathcal{C}_{2,1}^{\frac{1}{2}}\|_F^2 + \|\mathcal{C}_{2,2}^{\frac{1}{2}}\|_F^2)} \\ &= \sqrt{(n-r)\eta^2 n_b \sum_{i=\kappa+1}^n -\frac{1}{2\lambda_i}}. \end{aligned}$$

Inserting this along with P_* to the RHS of (52) yields the error bound (28).

D. Proof of Lemma VI.3

Denote $n_i = |\mathcal{I}_i|_c$, $i = 1, \dots, r$, the objective function of (opt2) can be expanded as

$$\bar{v}^T P^T \tilde{Q} P \bar{v} = \bar{v}^T P^T P Q P^T P \bar{v} = (w * w)^T (Q * \bar{v} \bar{v}^T) (w * w)$$

where $*$ is the Khatri-Rao product defined by

$$Q * \bar{v} \bar{v}^T = \begin{bmatrix} Q_{\mathcal{I}_1, \mathcal{I}_1} \otimes \bar{v}_{\mathcal{I}_1} \bar{v}_{\mathcal{I}_1}^T & \cdots & Q_{\mathcal{I}_1, \mathcal{I}_r} \otimes \bar{v}_{\mathcal{I}_1} \bar{v}_{\mathcal{I}_r}^T \\ \vdots & \ddots & \vdots \\ Q_{\mathcal{I}_r, \mathcal{I}_1} \otimes \bar{v}_{\mathcal{I}_r} \bar{v}_{\mathcal{I}_1}^T & \cdots & Q_{\mathcal{I}_r, \mathcal{I}_r} \otimes \bar{v}_{\mathcal{I}_r} \bar{v}_{\mathcal{I}_r}^T \end{bmatrix},$$

$$w * w = [w_{\mathcal{I}_1}^T \otimes w_{\mathcal{I}_1}^T \ \cdots \ w_{\mathcal{I}_r}^T \otimes w_{\mathcal{I}_r}^T]^T.$$

Denote the block-diagonal submatrix of Q by Q_d , i.e.

$$Q_d = \begin{bmatrix} Q_{\mathcal{I}_1, \mathcal{I}_1} & & \\ & \ddots & \\ & & Q_{\mathcal{I}_r, \mathcal{I}_r} \end{bmatrix},$$

and the off-diagonal by $Q_o = Q - Q_d$. Then, we have the objective function of (opt*) as

$$(w * w)^T [\Phi * \Phi + \rho Q * \bar{v} \bar{v}^T - \rho Q_o * \bar{v} \bar{v}^T] (w * w),$$

which equals to the objective function in (opt3) minus $(w * w)^T (\rho Q_o * \bar{v} \bar{v}^T) (w * w)$. According to the Gershgorin circle theorem, the eigenvalues of $\rho Q_o * \bar{v} \bar{v}^T$ are all bounded inside the range of $(-\| \rho Q_o * \bar{v} \bar{v}^T \|_1, \| \rho Q_o * \bar{v} \bar{v}^T \|_1)$. Therefore, the approximated optimization would yield a worst-case error as in (32), with $J_e = \| \rho Q_o * \bar{v} \bar{v}^T \|_1$.

REFERENCES

- [1] D. D. Siljak, *Decentralized Control of Complex Systems*, Courier Corporation, 2011.
- [2] P. Kokotovic, H. K. Khalil, and J. O'Reilly, *Singular Perturbation Methods in Control: Analysis and Design*, SIAM, 1999.
- [3] J. Chow and P. Kokotovic, "Time Scale Modeling of Sparse Dynamic Networks," *IEEE Transactions on Automatic Control*, vol. 30(8), pp. 714-722, 1985.
- [4] B. Moore, "Principal Component Analysis in Linear Systems: Controllability, Observability, and Model Reduction," *IEEE Transactions on Automatic Control*, vol. 26(1), pp. 17-32, 1981.
- [5] G. Obinata and B. D. Anderson, *Model Reduction for Control System Design*, Springer Science & Business Media, 2012.
- [6] A. C. Antoulas, *Approximation of Large-Scale Dynamical Systems*, SIAM, 2005.
- [7] K. Zhou and J. C. Doyle, *Essentials of Robust Control*, vol. 180, Prentice Hall Upper Saddle River, NJ, 1998.
- [8] A. Rahmani, M. Ji, M. Mesbahi, and M. Egerstedt, "Controllability of Multi-Agent Systems from a Graph-Theoretic Perspective," *SIAM Journal on Control and Optimization*, vol. 48(1), pp. 162-186, 2009.
- [9] H. G. Tanner, "On the Controllability of Nearest Neighbor Interconnections," *43rd IEEE Conference on Decision and Control (CDC)*, vol. 3, pp. 2467-2472, 2004.
- [10] A. M. Boker, T. R. Nudell, and A. Chakraborty, "On Aggregate Control of Clustered Consensus Networks," *2015 American Control Conference (ACC)*, pp. 5527-5532, Chicago, IL, USA, 2015.
- [11] S. Hara, J. I. Imura, K. Tsumura, T. Ishizaki, and T. Sadamoto, "Glocal (Global/Local) Control Synthesis for Hierarchical Networked Systems," *2015 IEEE Conference on Control Applications (CCA)*, pp. 107-112, Sydney, NSW, 2015.
- [12] T. Sadamoto, T. Ishizaki, and J. I. Imura, "Hierarchical Distributed Control for Networked Linear Systems," *53rd IEEE Conference on Decision and Control*, pp. 2447-2452, 2014.
- [13] D. Madjidian and L. Mirkin, "Distributed Control with Low-Rank Coordination," *IEEE Transactions on Control of Network Systems*, vol. 1(1), pp. 53-63, March 2014.
- [14] S. Lloyd, "Least Squares Quantization in PCM," *IEEE Transactions on Information Theory*, vol. 28(2), pp. 129-137, Mar 1982.
- [15] L. Qi, F. Wang, and Y. Wang, "Z-Eigenvalue Methods for a Global Polynomial Optimization Problem," *Mathematical Programming*, vol. 118, pp. 301-316, 2009.
- [16] F. Lin, M. Fardad, and M. R. Jovanovic, "Design of Optimal Sparse Feedback Gains via the Alternating Direction Method of Multipliers," *IEEE Transactions on Automatic Control*, vol. 58(9), pp. 2426-2431, Sep 2013.
- [17] N. Monshizadeh, H. L. Trentelman, and M. K. Camlibel, "Projection-Based Model Reduction of Multi-Agent Systems using Graph Partitions," *IEEE Transactions on Control of Network Systems*, vol. 1(2), pp. 145-154, Jun 2014.
- [18] T. Ishizaki, K. Kashima, A. Girard, J. Imura, L. Chen, and K. Aihara, "Clustered Model Reduction of Positive Directed Networks," *Automatica*, vol. 59, pp. 238-247, 2015.
- [19] P. Benner and Z. Bujanovi, "On the Solution of Large-Scale Algebraic Riccati Equations by Using Low-Dimensional Invariant Subspaces," *Linear Algebra and its Applications*, vol. 488, pp. 430-459, 2016.
- [20] M. Rotkowitz and S. Lall, "A Characterization of Convex Problems in Decentralized Control," *IEEE Transactions on Automatic Control*, vol. 51(2), pp. 274-286, Feb. 2006.
- [21] X. Wu and M. R. Jovanovic, "Augmented Lagrangian Approach to Design of Structured Optimal State Feedback Gains," *IEEE Transactions on Automatic Control*, vol. 56, pp. 2923-2929, Dec 2011.
- [22] Y. S. Wang, N. Matni, and J. C. Doyle, "Localized LQR Optimal Control," *53rd IEEE Conference on Decision and Control*, pp. 1661-1668, 2014.
- [23] Y. S. Wang and N. Matni, "Localized LQG Optimal Control for Large-Scale Systems," *2016 American Control Conference (ACC)*, pp. 1954-1961, Boston, MA, USA, 2016.
- [24] N. Xue and A. Chakraborty, " \mathcal{H}_2 -Clustering of Closed-Loop Consensus Networks under Generalized LQR Designs," *55th IEEE Conference on Decision and Control*, pp. 5116-5121, Las Vegas, NV, Dec 2016.
- [25] S. Fattahi, G. Fazelnia and J. Lavaei, "Transformation of Optimal Centralized Controllers into Near-Global Static Distributed Controllers," *53rd IEEE Conference on Decision and Control*, pp. 4915-4922, 2015.
- [26] A. Helmy, "Architectural Framework for Large-Scale Multicast in Mobile Ad Hoc Networks," *IEEE International Conference on Communications*, pp. 2036-2042, vol.4, 2002.
- [27] D. M. Cardoso, C. Delorme, and P. Rama, "Laplacian Eigenvectors and Eigenvalues and Almost Equitable Partitions," *European Journal of Combinatorics*, vol. 28, pp. 665-673, 2007.
- [28] J. N. Franklin, *Matrix Theory*, Courier Corporation, 2012.
- [29] R. Davies, P. Shi, and R. Wiltshire, "New Lower Solution Bounds of the Continuous Algebraic Riccati Matrix Equation," *Linear Algebra and Its Applications*, vol. 427(2-3), pp. 242-255, 2007.
- [30] G. H. Golub and C. F. Van Loan, *Matrix Computations*, JHU Press, vol. 3, 2012.
- [31] M. S. Traiantafyllou and F. S. Hover, *Maneuvering and Control of Marine Vehicles*, Cambridge, MA, 2002.
- [32] J. Sun, "Perturbation Theory for Algebraic Riccati Equations," *SIAM Journal on Matrix Analysis and Applications*, vol. 19, pp. 39-65, 1998.
- [33] E. Kofidis and P. A. Regalia, "On the Best Rank-1 Approximation of Higher-Order Supersymmetric Tensors," *SIAM Journal on Matrix Analysis and Applications*, vol. 23, pp. 863-884, 2002.

Nan Xue (S'15) received his B.E. degree in Electrical Engineering from Xi'an Jiaotong University, China in 2013. He is currently pursuing his PhD degree in Electrical Engineering at North Carolina State University, Raleigh, NC. His research interests include analysis, control and model reduction of large-scale networked dynamic systems and power systems.

Aranya Chakraborty (M'08, SM'15) received his PhD degree in Electrical Engineering from Rensselaer Polytechnic Institute, Troy, NY in 2008. From 2008 to 2009 he was a postdoctoral research associate at the Aeronautics and Astronautics department of University of Washington, Seattle. He is currently an Associate Professor in the Electrical and Computer Engineering department of North Carolina State University, Raleigh, NC, where he is also affiliated to the FREEDM Systems Center. His research interests are in all branches of control theory with applications to power systems, especially in wide-area monitoring and control of large power systems using Synchrophasors. He received the NSF CAREER award in 2011.